

THE LIFETIME AND POWERS OF FR IIS IN GALAXY CLUSTERS

JOE ANTOGNINI¹, JONATHAN BIRD^{1,2}, AND PAUL MARTINI^{1,2}

(Dated: June 20, 2018)
Draft version June 20, 2018

ABSTRACT

We have identified and studied a sample of 151 FR IIs found in brightest cluster galaxies (BCGs) in the MaxBCG cluster catalog with data from FIRST and NVSS. We have compared the radio luminosities and projected lengths of these FR IIs to the projected length distribution of a range of mock catalogs generated by an FR II model and estimate the FR II lifetime to be 1.9×10^8 yr. The uncertainty in the lifetime calculation is a factor of two, due primarily to uncertainties in the ICM density and the FR II axial ratio. We furthermore measure the jet power distribution of FR IIs in BCGs and find that it is well described by a log-normal distribution with a median power of 1.1×10^{37} W and a coefficient of variation of 2.2. These jet powers are nearly linearly related to the observed luminosities, and this relation is steeper than many other estimates, although it is dependent on the jet model. We investigate correlations between FR II and cluster properties and find that galaxy luminosity is correlated with jet power. This implies that jet power is also correlated with black hole mass, as the stellar luminosity of a BCG should be a good proxy for its spheroid mass and therefore the black hole mass. Jet power, however, is not correlated with cluster richness, nor is FR II lifetime strongly correlated with any cluster properties. We calculate the enthalpy of the lobes to examine the impact of the FR IIs on the ICM and find that heating due to adiabatic expansion is too small to offset radiative cooling by a factor of at least six. In contrast, the jet power is approximately an order of magnitude larger than required to counteract cooling. We conclude that if feedback from FR IIs offsets cooling of the ICM, then heating must be primarily due to another mechanism associated with FR II expansion.

Subject headings: cooling flows — galaxies: active — galaxies: clusters: general — galaxies: evolution — galaxies: jets

1. INTRODUCTION

It has long been known that fewer extremely high-mass galaxies are observed than simple, theoretical calculations predict (White & Frenk 1991). As random overdensities from the big bang collapse, hot gas in the largest overdensities cools and condenses toward their centers to form the progenitors of brightest cluster galaxies (BCGs). In the absence of any source of heating, gas from the protocluster will continue to radiatively cool onto the BCG at rates as high as $\sim 1000 M_{\odot} \text{ yr}^{-1}$ in so-called “cooling flows” (see Fabian 1994 for a review). However, X-ray observations indicate that the gas infall rate at the centers of most clusters is about 10% of that predicted by cooling flow models (Peterson et al. 2001; Tamura et al. 2001).

It is clear that some mechanism heats gas on the cluster scale roughly isotropically (see McNamara & Nulsen 2007 for a recent review). The best candidate is some form of radio-mode feedback. Since BCGs tend to be disproportionately radio-loud, it has been suggested that most BCGs go through a radio-loud phase (Burns 1990; Best et al. 2005). In this phase an AGN emits two radio jets which inflate large ($\sim 100 - 1000$ kpc), overpressured lobes in the intracluster medium (ICM). These radio lobes are often spatially coincident with X-ray cavities, implying that they physically displace and inject substantial energy into some regions of the ICM (Fabian et al. 2000; McNamara et al. 2000). The power required to inflate these cavities appears to be sufficient to counteract cooling of the hot gas (Birzan et al. 2004; Rafferty et al. 2006). Nev-

ertheless, it remains unclear how this energy heats the ICM sufficiently isotropically. Shocks and sound waves associated with the expansion of the lobe can transfer some heat from the lobe to the general ICM (Jones et al. 2002; Forman et al. 2005; Fabian et al. 2005) as could cosmic ray diffusion from the lobes (Mathews 2009). Conduction can ameliorate this problem to some extent, but to properly estimate the heating due to conduction requires detailed magnetohydrodynamic simulations (Dolag et al. 2004).

Large, extended radio sources have been well-studied for many decades. An early morphological classification scheme of double-lobed radio sources was developed by Fanaroff & Riley (1974). Core-brightened sources are classified as Type I sources (FR Is) and edge-brightened sources are classified as Type II sources (FR IIs). Although the classification is purely morphological, FR IIs are generally more luminous than FR Is. The jet power supplied by the AGN is believed to play an important role in the FR I/II dichotomy, but the occasional cases of “hybrid” sources which exhibit one FR I lobe and one FR II lobe indicate that environmental factors are not negligible (e.g., Gopal-Krishna & Wiita 2000).

Because FR IIs have sharp edges, many important properties (e.g., projected length, axial ratio, and luminosity) are well defined and independent of the sensitivity of the observation. By contrast, FR Is exhibit long plumes of fading radio emission, so properties like the length and total luminosity are more dependent on the sensitivity of the observation. FR IIs are therefore easier to study as probes of AGN activity and their effects on the ICM with radio observations alone. Furthermore, the advance speeds and axial ratios of FR IIs are similar across several orders of magnitude in lobe length, indicating that FR II evolution is approximately self-similar. This inference has addition-

¹ Department of Astronomy, The Ohio State University, 140 W 18th Ave., Columbus, Ohio 43210, USA

² Center for Cosmology & Astroparticle Physics, The Ohio State University, 191 W Woodruff Ave., Columbus, Ohio 43210, USA
Electronic address: antognini@astronomy.ohio-state.edu

ally been supported by more detailed hydrodynamical simulations (Carvalho & O’Dea 2002a,b). The assumption of self-similarity has allowed the possibility of analytical or semi-analytical models to describe FR II evolution. A number of such models have been developed over the past two decades. Among the most complete and most widely used is the model presented in Kaiser & Alexander (1997) and Kaiser, Dennett-Thorpe, & Alexander (1997), henceforth referred to as the KDA model. We use the KDA model exclusively throughout this paper.

The calculation of the length evolution of the lobe is straightforward and is similar in all FR II models. Earlier FR II studies have used FR II lobe length distributions to estimate FR II ages of 10^7 to 10^8 years (Blundell et al. 1999; Bird et al. 2008). These measurements are in reasonable agreement with spectral aging estimates and measurements of the buoyant rising times of ghost cavities, which find FR II ages in the range of 10^6 to 10^8 yr (Allen et al. 2006; O’Dea et al. 2009). These estimates generally only reflect the current age of individual sources, or subsets of the population that may not be representative, and do not provide a direct estimate of the lifetime or energy of typical sources. While it is possible to infer an FR II lifetime from an age distribution, it requires good knowledge of the selection efficiency as a function of age. Studies which attempt to infer the FR II lifetime from length distributions can constrain their selection biases more easily (Blundell et al. 1999; Bird et al. 2008), but still suffer from uncertainties in the jet power.

The FR II jet power is a difficult quantity to determine and the few FR IIs for which it has been estimated have tended to be unusually bright, and hence, high-power sources (Machalski et al. 2004; McNamara & Nulsen 2007). Inferring the general FR II jet power distribution from the high-power end alone, however, requires substantial and uncertain extrapolation. Nevertheless, recent studies have begun to probe the low-power end of the FR II jet power distribution and have found typical jet powers of 10^{37} W and jet powers as low as 10^{36} W (Cavagnolo et al. 2010; Ito et al. 2008; Punsly & Zhang 2011). These estimates place the median FR II power lower than older estimates by at least an order of magnitude. Although FR II lifetime estimates do not scale sensitively with FR II power, a substantial overestimate of the jet power will lead to an underestimate of the age or lifetime.

In this work we measure the ages and powers of 151 FR IIs in BCGs from the MaxBCG galaxy cluster catalog of Koester et al. (2007a). We simultaneously fit the length and luminosity of the FR IIs with the KDA model and derive an estimate of the power distribution. We then obtain an improved lifetime and duty cycle estimate and examine the importance of FR IIs in ICM heating. The paper is organized as follows: in §2 we describe the sample selection algorithm, the luminosity and projected length measurements, and list general properties of the FR IIs in our sample; in §3 we motivate our use of the KDA model, provide a summary of the model’s important features, and describe our technique to estimate the jet powers; in §4 we fit the observed length distribution to a set of mock catalogs generated by a Monte Carlo simulation of FR II observations; in §5 we investigate correlations between FR II power and lifetime with various cluster properties and examine the FR II fraction as a function of cluster properties; in §6 we compare our results with those in the literature and discuss the heating effects of FR IIs on the ICM; we summarize our results in §7.

Throughout the paper we assume a Λ CDM cosmology with

$$\Omega_m = 0.27, \Omega_\Lambda = 0.73, \text{ and } H_0 = 70 \text{ km s}^{-1} \text{ Mpc}^{-1}.$$

2. SAMPLE SELECTION

Our sample selection process is similar to the process used in Bird et al. (2008), namely we identify FR IIs hosted by central galaxies in dense environments. The major difference is that we use the MaxBCG catalog of Koester et al. (2007a) to identify BCGs rather than the catalog of galaxy groups published by Berlind et al. (2006). We describe properties of the galaxy cluster catalog in §2.1 and properties of the catalogs of radio sources in §2.2. Our process for cross-correlating the two catalogs is described in §2.3. §2.4 describes the sample selection method and properties of the final FR II sample.

2.1. Cluster Catalog

The MaxBCG catalog consists of 13,823 galaxy clusters selected from the Sloan Digital Sky Survey with the maxBCG red-sequence method. The red sequence method attempts to find BCGs by selecting galaxies lying on the E/S0 ridge-line (a region of color-magnitude space where old, passively evolving galaxies are found) which are also brighter than their neighboring galaxies. The algorithm identifies potential BCGs in an overdensity of galaxies with similar colors and redshifts. The red sequence method is described in detail in Koester et al. (2007a). Tests using mock catalogs performed by Koester et al. (2007b) indicate that the MaxBCG catalog is at least 90% pure and 85% complete for clusters larger than $10^{14} M_\odot$.

The number of galaxies with similar colors and redshifts in the overdense region, N_{gal} , is an estimate of the total number of galaxies in the cluster. N_{gal} is later refined to N_{gal}^{R200} , the number of galaxies within the radius at which the galaxy density is 200 times larger than the mean density of galaxies with $-24 \leq M_r \leq -16$ mag. Throughout this paper we use N_{gal}^{R200} as a proxy for the cluster richness.

The MaxBCG cluster catalog spans a range in photometric redshift of $z = 0.1 - 0.3$ and a range in richness of $N_{\text{gal}}^{R200} = 10 - 188$. 39% of the BCGs in the MaxBCG catalog also have spectroscopic redshifts and the dispersion between the spectroscopic and photometric redshifts is 0.01. Throughout this paper we use spectroscopic redshifts whenever they exist and otherwise use photometric redshifts. The distribution of cluster richness and redshifts in the MaxBCG catalog is shown in Figure 1.

Although the MaxBCG catalog does not provide cluster mass estimates, the clusters span a range of r -band luminosity from $7 \times 10^{10} L_\odot$ to $3 \times 10^{12} L_\odot$ with a median luminosity of $2 \times 10^{11} L_\odot$. For a typical cluster mass-to-light ratio of $\sim 350 M_\odot / L_\odot$ (Carlberg et al. 1997; Sheldon et al. 2009), the typical cluster mass in the MaxBCG catalog is $\sim 7 \times 10^{14} M_\odot$ with a spread of about one order of magnitude in either direction.

2.2. Radio Catalogs

We selected radio sources associated with the BCGs of these galaxy clusters using the July 16, 2008 version of the FIRST radio catalog (White et al. 1997). The FIRST radio catalog consists of 816,331 radio sources identified from 9055 deg^2 observed as part of the FIRST radio survey at 1.4 GHz (Becker et al. 1995). Data for this version of the catalog were obtained with the Karl G. Jansky Very Large Array (VLA) from 1993 through 2004. The angular resolution of the FIRST survey is $5''/4$ and the typical rms flux noise is 0.15 mJy. Dirty

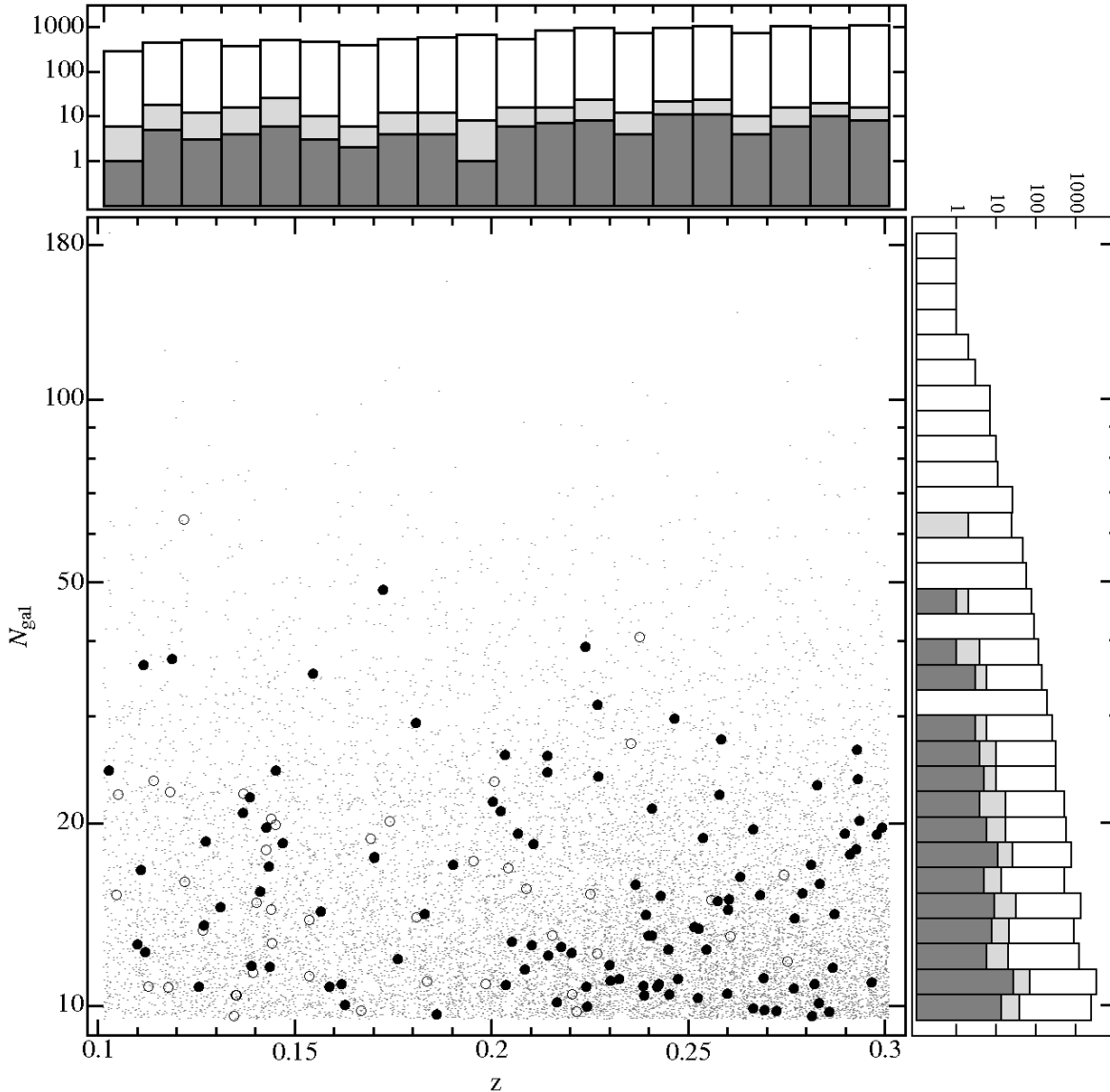


FIG. 1.— The distribution of cluster richness and redshift in the MaxBCG catalog (small gray points), the full FR II sample (large open and filled circles), and the volume-limited FR II sample (filled circles alone). Histograms of the cluster richness and redshift are also shown. The unfilled area represents the counts for all clusters in the MaxBCG catalog, the light gray area the counts for those clusters with FR IIs in our full sample, and the dark gray area the counts for those clusters with FR IIs in our volume-limited sample.

beams from the VLA were CLEANed to produce images for the FIRST survey with $1''.4$ pixels.

The FIRST radio catalog was produced from the survey data using a specialized source extraction algorithm dubbed HAPPY. HAPPY searches for local maxima and attempts to fit them to up to four elliptical Gaussian components. Fits which produce physical results and are not too close to an image edge are accepted into the catalog. The catalog is then refined to eliminate duplicate and spurious sources. To be considered a detection, a source must be at least five times larger than the rms noise. The minimum flux of any source is therefore typically above 0.75 mJy.

The resulting catalog provides, among other parameters, the coordinates, the local rms noise, the peak and integrated flux, and a warning flag if the source is a potential sidelobe of a nearby bright source. The two flux measurements are corrected for CLEAN bias (Becker et al. 1995; Condon et al. 1998).

Because the FIRST survey has relatively high resolu-

tion and treats extended sources as collections of point-like sources, much of the flux of extended objects can be resolved out and missed, thereby leading to underestimates of the total flux. Since FR IIs are extended, we complement our flux measurements of sources from the FIRST catalog using the NRAO VLA Sky Survey (NVSS). NVSS is a similar radio survey to FIRST, but has an angular resolution of $45''$ rather than $5''.4$, thereby providing more accurate flux measurements for extended sources (Condon et al. 1998). The flux limit for the NVSS catalog is $S \simeq 2.5$ mJy. Although this is larger than FIRST by a factor of approximately three, extended sources are broken into fewer components in the NVSS catalog and we lose no FR IIs in the NVSS catalog.

2.3. Cross-Correlating the Two Catalogs

We first selected a sample of FR II candidates by identifying radio sources between $10''.8$ and $3.4'$ of every BCG. The upper bound of $3.4'$ was chosen to be small enough to limit the number of spurious candidates, yet large enough that real FR IIs

would not be eliminated. At a redshift of $z = 0.1$, the lowest in our sample, this cut would eliminate any FR IIs longer than 370 kpc. Since we found no FR IIs longer than 287 kpc, we conclude that this choice of maximum angular separation has no effect on our sample size. The lower bound of $10''8$ was chosen so that the FR IIs would be at least a factor of two greater than the FIRST resolution. The selection function for short FR IIs near the FIRST resolution limit is difficult to characterize; some FR IIs near the FIRST resolution limit were discovered by our selection algorithm, whereas others, due to the chance peculiarities of their morphology or surroundings, may have been missed. By selecting only FR IIs whose lobes each subtend at least two resolution elements of FIRST, we ensure that our selection algorithm only identifies FR IIs that are resolved by FIRST.

Except in rare cases when a radio jet is oriented very nearly along the line of sight and has one lobe strongly beamed towards the Earth and the other lobe strongly beamed away, radio jets appear to be extremely symmetrical (Scheuer 1995). We thus identified FR II candidates as radio sources that were equidistant from the central BCG to within 30% and at least 135° away from each other relative to the BCG. These selection criteria yielded an initial sample of 617 FR II candidates. We then superimposed FIRST contours on SDSS images of these FR II candidates and inspected them by eye to eliminate contaminants. There were two major sources of contamination: (1) pairs of radio galaxies on opposite sides of the BCG or (2) a radio galaxy paired with a faint radio source unassociated with any optical counterpart. Aside from their spatial coincidence with optical sources, contaminants in both cases could be easily distinguished from faint FR II lobes due to the relatively large asymmetry between the position of the two sources with respect to the BCG, the relatively large asymmetry in flux, and the lack of any extended emission toward the BCG. We also removed 31 obvious FR Is from the sample. This resulted in a preliminary sample of 432 FR IIs. Less-obvious FR I sources were removed in a more quantitative second pass described in the following section.

2.4. FR II Classification and Sample Selection

Although FR Is can often be distinguished from FR IIs based on luminosity alone, the formal division between FR I and FR II sources is purely morphological (Fanaroff & Riley 1974). Sources for which the hotspot is closer to the tip of the lobe are classified as FR IIs, and sources for which the hotspot is closer to the central galaxy are classified as FR Is. Except in extreme cases, since projection effects cannot drastically change the ratio between the distance to the hotspot and the distance to the lobe tip, the projected positions of the hotspot, lobe tip, and central galaxy are sufficient to eliminate any remaining FR Is from our sample.

We therefore measured the position of the hotspot and the tip of the lobe for each FR II in the sample. We identified the position of the hotspot as the centroid at the local maximum near the FR II's edge. It is inherently more difficult to determine the tip of the lobe. Although the lobes of FR II sources have better-defined edges relative to FR Is, the tip of a lobe is nevertheless not entirely well-defined due to variations in the sensitivity of the radio data and the often complex morphology of the source. We defined the tip of the lobe as the most distant pixel from the central BCG that was contiguous with the main lobe and above the FIRST detection threshold by five times the rms noise. Once we determined the position of the hotspot and tip of the lobe, we removed less-evident

FR Is from the sample.

We derive the projected physical length of each source from the separation of each lobe tip from the BCG and the angular diameter distance to the cluster. The errors on the projected source sizes are dominated by random errors in the photometric redshift and the uncertainty in the definition of the lobe tip. We estimate that the total uncertainty in the physical lobe length is $\lesssim 5\%$. As shall be shown in §§4.2 and 4.3, the uncertainty in our lifetime calculation is dominated by uncertainty in the ICM and the FR II model, rather than the uncertainty in physical lobe length.

We obtained the fluxes for the FR IIs from the NVSS catalog. Because NVSS, like FIRST, breaks up extended sources into discrete components, the flux from each component was summed to give the total flux from each side of the FR II source. Since NVSS cannot resolve the double-lobed morphology of the smaller sources in the sample, it was often impossible to assign a separate flux to each lobe. In these instances we measured the total flux from both lobes. When fluxes from individual lobes were needed, such as when estimating the power and age of the jet as described in §3.3, we simply assigned each lobe half the total flux. Since this prescription requires that both lobes be FR IIs, we made a final cut in our sample to eliminate any radio sources that consisted of an FR II lobe paired with an FR I lobe. This cut eliminated 42 nominal FR I/II mixed sources. We note that the vast majority of these mixed sources are not “true” FR I/II hybrid sources in the usual sense of a well-defined FR I plume on one side and a well-defined FR II lobe on the other (so-called “HYMOR” sources, Gopal-Krishna & Wiita 2000). Rather, in these sources the hotspots of both lobes are approximately halfway along the length of the lobe and one hotspot is slightly beyond halfway to the lobe tip and the other slightly before. Application of all of these selection criteria resulted in a flux-limited sample of 151 FR II lobe pairs. We perform the bulk of analysis with this sample and will simply refer to it as “the sample” or the “full sample” rather than the flux-limited sample. The distribution of the FR IIs in our sample in redshift and host cluster richness is shown in Figure 1 and the projected length distribution is shown in Figure 2.

This sample of 151 FR II lobe pairs suffers from several significant selection biases. Specifically, intrinsically longer jets are easier to resolve at larger distances, and more luminous FR IIs are easier to detect at larger distances. Since more powerful FR IIs are both longer and more luminous at a given age than less powerful FR IIs (Kaiser et al. 1997), this sample is biased towards more powerful FR IIs at higher redshifts. These biases become problematic when attempting to determine whether FR II lifetime or duty cycle change with redshift. To ameliorate this problem, we introduced a cut into our sample that required every FR II source meet our selection criteria at $z = 0.3$, the largest redshift of the clusters in our sample. That is, if the source were at $z = 0.3$, the angular separation between the two lobes of the jet would have to be at least $10''8$, and the flux from the FIRST component for both hotspots would have to be above the FIRST detection limit of five times the rms background noise. There are 108 pairs of FR II lobes in this sample, which we will refer to as the volume-limited sample. The length distribution of the volume-limited sample is also shown in Figure 2.

There is likely a slight overcorrection in the volume-limited sample, but one that is difficult to quantify. Because extended sources appear more compact at larger distances, high-resolution surveys like FIRST can collect more flux from the

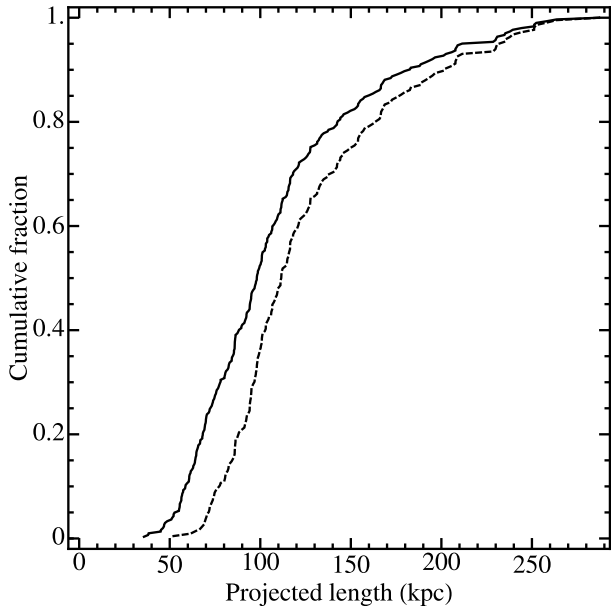


FIG. 2.— The length distribution of the full (solid line) and the volume-limited (dashed line) FR II samples. Since shorter sources are not resolved by FIRST at high redshifts, the volume-limited sample contains fewer short FR IIs than the flux-limited sample.

source. Thus if an extended source at $z < 0.3$ is moved out to $z = 0.3$, the flux detected by FIRST would be slightly larger than one would expect based on the change in distance alone. Since this effect is difficult to characterize accurately due to the complex morphology of the sources, we simply note that low-redshift sources in our volume-limited sample are slightly biased towards larger lengths.

The properties of all of the FR II sources and their host clusters are listed in Table 1. Figure 3 displays examples of several randomly selected FR IIs from our sample and Figure 4 presents a P - D diagram of the full sample. The sources span a range of lengths of 48–287 kpc with a median length of 95 kpc. The host clusters span a range of richness from 10 (the minimum richness in the MaxBCG catalog) to 69 with a median richness of 14 and the full redshift range of the MaxBCG catalog of $z = 0.1$ – 0.3 . The sample spans a range in specific luminosity of 4.4×10^{23} – 7.2×10^{25} $\text{W m}^{-2} \text{Hz}^{-1}$ with a median luminosity of 8.0×10^{24} $\text{W m}^{-2} \text{Hz}^{-1}$ (all at an observed frequency of 1.4 GHz). Note that we do not K -correct the luminosities of the FR II sample at this point, but account for K -corrections in the mock catalogs (described in §3.5).

These luminosities are smaller by at least an order of magnitude than the luminosities of FR II sources in many earlier studies (e.g., Laing et al. 1983; Subrahmanyam et al. 1996; Cotter et al. 1996) and are smaller than the luminosities of well-studied FR IIs like Cygnus A, 3C 47, and 3C 295 by over three orders of magnitude (Braude et al. 1969). Indeed, 75% of the sources in our sample fall below the FR I/II demarcation line set out in Ledlow & Owen (1996). While it is possible that some sources close to our resolution cutoff may be FR Is confused for FR IIs, the vast majority of our sources are well resolved. Specifically, $\sim 75\%$ of our sample has an angular separation of at least three FIRST beams, $\sim 50\%$ of our sample has an angular separation of at least four FIRST beams, and $\sim 25\%$ of our sample has an angular separation of at least six FIRST beams.

The relatively low luminosity of the FR IIs in our sample is due to the FIRST survey’s superior sensitivity and resolution with respect to earlier radio surveys. Probing the faint end of

the FR II luminosity function allows us to better constrain the lower-limit of FR II jet power and study the characteristics of more typical FR IIs. We address this subject in detail in §3.3.

3. MODELING THE LENGTH DISTRIBUTION

We estimate the lifetime and jet powers of FR IIs with detailed models of their luminosity evolution, environments, and the sample selection. This approach requires a good model of FR II length and luminosity evolution, and our choice is discussed in §3.1. The model for the ICM can impact the lifetime determination as well, so we discuss the properties of the ICM models we use in §3.2. In §3.3 we introduce the method by which we estimate FR II jet powers, a major contribution to the uncertainty in previous FR II lifetime measurements. We present a relationship between the jet power and the radio luminosity in §3.4. We finally discuss our use of mock catalogs to account for selection effects in §3.5.

3.1. Properties of the FR II Model

To determine the FR II source lifetime we need an accurate, analytic model of the length and luminosity evolution of the sources. A number of analytic models of FR II source evolution exist in the literature (e.g., Bicknell et al. 1997; Kaiser et al. 1997; Blundell et al. 1999; Manolakou & Kirk 2002; Kino & Kawakatu 2005). The Bicknell, KDA, Blundell, and Manolakou models all assume self-similar growth of the jet. Although this assumption appears to be approximately correct, hydrodynamical simulations by Carvalho & O’Dea (2002a,b) show that it fails in detail in low Mach number jets in ICMs with relatively flat density profiles. The more recent model by Kino & Kawakatu (2005) avoids the assumption of self-similarity, although it only describes the total kinetic power rather than the radio luminosity of the source. Since the density profile of the ICM of galaxy clusters tends to be steep and the jets in FR IIs have large Mach numbers, the self-similarity assumption is not problematic for our purposes. The radio luminosity of the FR II sources plays an important role in our determination of their lifetimes, so we find the Kino model to be unsuitable for our study. Barai & Wiita (2006) compared the Bicknell, Manolakou, and KDA models to FR II radio galaxies in the 3CRR, 6CE, and 7CRS radio surveys and found that the KDA model best matched data in the P - D - z - α plane. Based on this result, and for purposes of comparison with a similar study by Bird et al. (2008), we use the KDA model to describe the length and luminosity evolution of jets in our sample.

The KDA model was recently reworked into a simpler form by Kaiser & Best (2007); we adopt their notation for this paper. We note, however, that we have made one modification to the original KDA model. In a subsequent paper, Kaiser & Alexander (1999a) performed hydrodynamical simulations to test the accuracy of the KDA model. While the analytic model agreed with hydrodynamical simulations, Kaiser & Alexander found that an approximation made in Kaiser & Alexander (1997) of

$$\frac{p_h}{p_c} = A^2 \quad (1)$$

overestimates p_h/p_c , where p_h is the pressure at the head of the jet, p_c is the pressure within the cocoon, and A is the axial ratio. Kaiser (2000) provided an empirical parameterization of this ratio based on earlier simulations, giving

$$\frac{p_h}{p_c} = (2.14 - 0.52\beta) \left(\frac{A}{2}\right)^{2.04 - 0.25\beta}, \quad (2)$$

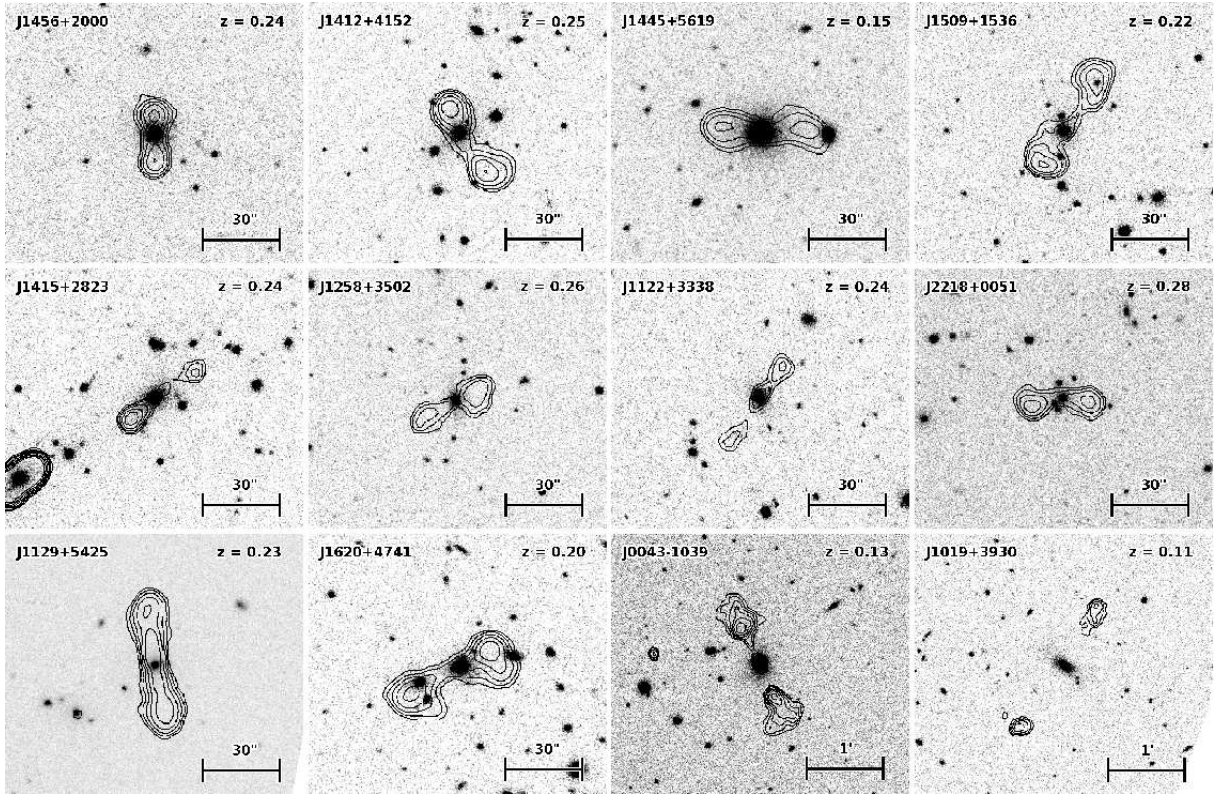


FIG. 3.— Twelve randomly chosen FR II radio sources from the sample. These are SDSS r -band images with contours from the FIRST survey superimposed.

TABLE 1
FR II SAMPLE

SDSS ID	z	N_{200}	L_r, BCG ($10^{10} L_\odot$)	L_z, BCG ($10^{10} L_\odot$)	F_{NVSS} (mJy)	P_{NVSS} ($10^{24} \text{ W Hz}^{-1}$)	l_1 (kpc)	l_2 (kpc)	l_1 (arcsec)	l_2 (arcsec)	In volume-limited sample?
(1)	(2)	(3)	(4)	(5)	(6)	(7)	(8)	(9)	(10)	(11)	(12)
J001247.6+004715.8	0.154	14	5.46	6.83	61.7	3.9	46.9	56.0	13.2	15.8	No
J003614.2-090451.8	0.270	10	4.43	5.24	17.0	3.8	121.0	127.8	18.1	19.1	Yes
J004312.9-103956.1	0.128	19	7.71	9.60	148.4	6.2	119.6	122.8	41.4	42.5	Yes
J013157.8-081955.0	0.140	11	7.51	9.65	469.0	24.2	55.5	85.9	17.3	26.8	No
J073826.2+451719.1	0.221	10	6.36	8.07	91.9	13.0	65.3	80.3	12.3	15.1	No
J074616.9+220203.5	0.260	19	6.16	7.51	30.4	6.2	86.1	110.1	13.5	17.2	Yes
J075457.8+210129.0	0.256	14	5.42	6.78	21.7	4.3	64.2	74.0	10.8	11.8	Yes
J075614.8+251340.4	0.202	11	8.67	10.77	188.8	21.7	75.5	111.1	15.7	23.2	Yes
J080107.0+175845.3	0.146	24	5.05	6.52	890.7	49.9	78.1	104.8	23.3	31.3	Yes
J080641.4+494628.4	0.245	13	5.90	7.66	84.2	15.0	84.9	112.4	14.2	18.8	Yes

NOTE. — FR II sources in our sample ordered by right ascension. (1): SDSS identifier. (2): BCG redshift. (3): Cluster richness. (4, 5): The r - and z -band luminosities of the BCG, respectively. (6): Total flux as measured by NVSS in mJy. (7): Specific radio luminosity of the FR II calculated from the NVSS flux in $10^{24} \text{ W Hz}^{-1}$. (8, 9): Projected length of the two lobes in kpc. (10, 11): Angular separation of the two lobes in arcseconds. (12): Identifies whether the FR II is also in the volume-limited sample. Table 1 is presented in its entirety in the electronic edition. A portion is shown here for guidance regarding its form and content.

where β is the power law slope of the ICM density profile. This modification has the following effect on the KDA model. The length of the lobe in the original KDA model is given by

$$D = c_1 \left(\frac{Q}{\rho a^\beta} \right)^{1/(5-\beta)} t^{3/(5-\beta)}, \quad (3)$$

where c_1 is

$$c_1 = \left[\frac{A^4 (\Gamma_x + 1)(\Gamma_l - 1)(5 - \beta)^3}{18\pi 9[\Gamma_l + (\Gamma_l - 1)A^2/2] - 4 - \beta} \right]^{1/(5-\beta)}, \quad (4)$$

t is the age of the FR II, Q is the jet power, and Γ_x and Γ_l are the adiabatic indices of the ICM and the lobe, respectively. By substituting Equation (1) for Equation (2), the constant c_1 becomes

$$c_1^{5-\beta} = \left(\frac{(2.14 - 0.52\beta)A^2}{18\pi} \left(\frac{A}{2} \right)^{2.04 - 0.25\beta} \right) \times \left(\frac{(\Gamma_x + 1)(\Gamma_l - 1)(5 - \beta)^3}{9[\Gamma_l + (\Gamma_l - 1)A^2/2] - 4 - \beta} \right). \quad (5)$$

For our choice of $\beta = 1.9$ (discussed in §3.2), this modifica-

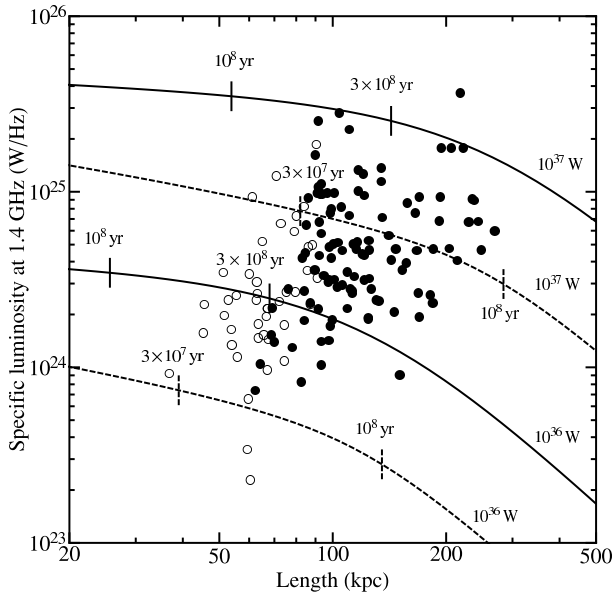


FIG. 4.— Radio luminosity vs. lobe length for FR IIs in the full (open and filled circles) and volume-limited samples (filled circles only). There is no clean line in length-luminosity space that divides the two samples because the sample cut was made with the length to the hotspot, while the length to the edge of the lobe is shown in this figure and the ratio between the hotspot and lobe distance can vary by up to a factor of two. For comparison, evolutionary tracks from the KDA model for four extreme cases are shown. The solid lines show an ICM model with $a = 260$ kpc and $\rho = 5.9 \times 10^{-24}$ kg/m³, characteristic of a rich cluster, and the dashed lines show an ICM model with $a = 2$ kpc and $\rho = 7.2 \times 10^{-22}$ kg/m³, characteristic of a small group. Both the upper solid and dashed lines represent a jet with a power of $Q = 10^{37}$ W, and the lower solid and dashed lines represent a jet with a power of $Q = 10^{36}$ W. The left and right ticks of the solid lines represent ages of 10^8 and 3×10^8 yr, respectively, and the left and right ticks of the dashed lines represent ages of 3×10^7 and 10^8 yr, respectively.

tion shortens the predicted lengths by approximately 40% and increases the age by approximately 70%.

The salient feature of the KDA model is that it predicts the source length and specific luminosity of a jet given an age, jet power, redshift, and a number of additional parameters that describe the jet’s shape and environment. The full list of inputs and several of the most relevant outputs of the KDA model is displayed in Table 2 along with the range over which we vary the parameters and our default values in this paper. Because the KDA model must be run several million times for a given choice of inputs in order to accurately model the length distribution, it is too computationally expensive to sample the entire range of parameter space that the KDA model offers. Bird et al. (2008) found, however, that most of the parameters have only a negligible impact on FR II lifetime calculations over physically plausible ranges. We therefore limit our exploration of parameter space to only those parameters which Bird et al. (2008) found to have a substantial impact on lifetime calculations, namely the density parameter ρa^β and the axial ratio A .

3.2. Treatment of the ICM

Apart from an assumption of self-similar growth, the KDA model also assumes that the ambient medium is described by a power-law profile of the form

$$\rho_x = \rho \left(\frac{r}{a} \right)^{-\beta}. \quad (6)$$

where a is the scale length of the distribution and ρ is the density at the scale length. As every other equation in the

KDA model involving ρ and a incorporates this one, these two parameters are not independent, but instead enter into the model only in their combined form, ρa^β (β , however, enters the model in separate equations and so is independent from a and ρ). Kaiser & Best (2007) term the product ρa^β the “density parameter” and we adopt that nomenclature in this paper.

The KDA model uses this simplified profile to make the calculation of more complicated quantities feasible, although at the expense of some shortcomings in the model. For example, while the KDA model adopts a density distribution for the ambient medium, there is no model for the pressure or the temperature. As a result, the KDA model tacitly assumes that the jet cocoon remains overpressured throughout its entire lifetime. Indeed, the KDA model requires that the lobe drive a strong shock into the external medium. Kaiser & Best (2007) point out that the pressure in the cocoon of an FR II source decreases over time, and argue that if the cocoon pressure falls below the ambient pressure at any point along the surface of the cocoon, Kelvin-Helmholtz instabilities will mix cooler gas from the external medium into the cocoon. This process would disrupt the jet and transform it into an FR I. If the pressure profile can be described by a flat core with a power-law tail, then low-power jets will become underpressured and transform into FR Is before escaping from the core region; however, more powerful jets will escape the core region and will remain overpressured (and hence FR IIs) for their entire lifetimes. With this model, Kaiser & Best (2007) present an order-of-magnitude calculation and find that the critical power is 3×10^{37} W.

Given the lengths of the FR IIs in our sample, the KDA model predicts that even FR IIs with this minimum power are much more luminous than the sources in our sample. As described next in §3.3, to reproduce jets with roughly the same lengths and luminosities as the jets in our sample, the KDA model requires that the typical jet power be over an order of magnitude smaller than the minimum FR II jet power power found by Kaiser & Best (2007). This would imply that the jets are underpressured prior to leaving the flat core of the ICM. There are two problems with this interpretation, however. The first is that a detailed examination of the pressure profiles of galaxy groups and clusters reveals that, while complex and varied in shape, they generally have cusps at their centers rather than flat cores (e.g., Vikhlinin et al. 2006). This suggests that many underpowered jets would start their lives as FR Is rather than later disrupting from FR IIs. Because the ICM density profiles measured by Vikhlinin et al. (2006) can vary substantially from one group or cluster to the next, there is likely no single, universal critical power. Furthermore, because the ICM profile can exhibit plateaus and bumps, it is difficult to predict whether an FR II will ever become underpressured, and if so, at what radius, without knowing the detailed ICM profile of a group or cluster. The second problem with the interpretation of the jets in our sample as underpressured is that the KDA model calculates the pressure at the head of the jet and assumes the pressure in the cocoon to be uniform. Disruption of the jet is likely to occur near the base of the jet, however, where the ICM pressure is greatest. Since the jet expansion speed can be comparable to, or even larger than, the sound speed within the cocoon, the pressure within the cocoon at the head of the jet will not necessarily be a good proxy for the pressure within the cocoon near the center of the FR II source, particularly towards the end of the jet’s life. Indeed, hydrodynamical simulations suggest that the pressure within the cocoon varies along and across the axis of

TABLE 2
INPUT & OUTPUT PARAMETERS OF THE KDA MODEL

Parameter type	Parameter	Default value	Minimum value	Maximum value	Description
Primary input	t	FR II age
Primary input	Q	Jet power
Primary input	z	Redshift
Secondary input	A	4.0	2.0	16.0	Axial ratio (see §4.2 for our definition of A)
Secondary input	ρ	$7.2 \times 10^{-26} \text{ kg m}^{-3}$	$7.2 \times 10^{-26} \text{ kg m}^{-3}$	$7.2 \times 10^{-22} \text{ kg m}^{-3}$	Density at a_0
Secondary input	a_0	391 kpc	2 kpc	391 kpc	Scale radius of ICM density profile
Secondary input	β	1.9	Power-law slope of ICM density profile
Secondary input	m	2.14	Power-law slope of injection energy of particles in jet
Secondary input	ν	1.4 GHz	Observation frequency
Secondary input	Γ_x	5/3	Adiabatic index of the ICM
Secondary input	Γ_l	4/3	Adiabatic index of the lobe
Secondary input	Γ_B	4/3	Adiabatic index of the magnetic field energy density
Secondary input	γ_{\min}	1	Minimum Lorentz factor for electrons in the jet
Secondary input	γ_{\max}	10^{10}	Maximum Lorentz factor for electrons in the jet
Secondary input	k	0	Ratio of energy stored in non-radiating particles to the sum of the energy in the magnetic field and the relativistic electrons.
Output	l	FR II Lobe length
Output	L	FR II radio luminosity
Output	p_c	FR II lobe pressure

NOTE. — We designate input parameters which are likely to be significantly different among FR IIs to be “Primary inputs” and therefore assign no default values to them. A similar study by Bird et al. (2008) found that variation of most of the secondary inputs does not substantially affect the result of the lifetime calculation. We therefore only varied those parameters which have a substantial effect on the lifetime calculation. Maximum and minimum values for parameters that we did not vary are given by ellipses.

an FR II jet and that the cocoon can become underpressured with respect to the ambient medium without disrupting the jet (Carvalho & O’Dea 2002b). Based on these considerations and our observations, we conclude that the minimum FR II jet power derived by Kaiser & Best (2007) is too high by at least an order of magnitude.

The density profile of the ICM in galaxy clusters is difficult to measure and the core density and scale radius can vary by several orders of magnitude (Mohr et al. 1999; Mulchaey 2000; Vikhlinin et al. 2006; Freeland & Wilcots 2011). Cotter (1996) and Kaiser et al. (1997) found that the power-law slope of the ICM density profiles in galaxy clusters hosting FR IIs are typically consistent with a value of $\beta = 1.9$. We adopt this slope throughout this paper. Larger values of β cannot support FR IIs (Falle 1991) and smaller values result in a smaller variation in the density parameter in different ICMs, thereby making our lifetime results less sensitive to the ICM properties. Bird et al. (2008) demonstrated in their appendix that the lifetimes of FR IIs depend upon the cube root of the density parameter, so a three order-of-magnitude variation in density parameter manifests itself as an order-of-magnitude uncertainty in the lifetime calculation of the jet. Although this dependence is weak, we note that quantities which depend on the volume of the lobe (e.g., the energy contained in the lobe) depend linearly on the density parameter.

Insufficient X-ray data exist to measure the ICM density profiles for these clusters. Instead we calculate the FR II lifetime separately for five different ICM density estimates drawn from the literature and then use optical richness as a proxy for ICM density in §5. To facilitate reference to each of the density estimates we label each with the symbol χ_i . These five density estimates are listed in full in Table 3 with references, but we describe them in order of increasing density parameter here as follows. χ_1 is the density assumed by Blundell et al. (1999), which was taken from Garrington & Conway (1991) and assumed to be typical of a poor group. χ_2 is the de-

fault density assumed by Kaiser et al. (1997) and was taken from Canizares et al. (1987), who also found it to be typical for poor groups. χ_3 was found by Jetha et al. (2007) to be typical for moderately sized groups and poor clusters (i.e. a typical richness of 9 – 12). χ_4 and χ_5 were measured by Jones & Forman (1984), who found them to be typical for moderately sized and massive clusters, respectively. These last two models were used by Kaiser & Alexander (1999b). These five estimates span three orders of magnitude and the full range of plausible density parameters for the host clusters of the FR IIs in our sample. We expect, however, that the Jetha et al. (2007) density estimate most closely approximates the ICM density of most of the host clusters in our sample since the clusters in our sample have a median richness which is comparable to the median richness of the Jetha et al. (2007) sample.³ We therefore take the χ_3 density model to be the default density model throughout this paper.

3.3. The Jet Power Distribution

In addition to an ICM model, the KDA model requires a jet power to calculate the length and luminosity as a function of age. To model the observed length distribution, we therefore require a plausible distribution of jet powers. Bird et al. (2008) used two power-law distributions, one from Blundell et al. (1999) and one derived from Sadler et al. (2002). Although the two distributions have very different slopes (0.62 and 2.6), they have similar median powers. Because the FR II length distribution depends primarily on the median power of the FR IIs, not powers at the tails of the distribution, Bird et al. (2008) found similar results with both distributions. We find both of these distributions to be unsuitable, however. If we use the KDA model to model a jet at

³ Although Jetha et al. (2007) do not cite richness estimates, compiling richnesses for clusters in their sample from various sources in the literature yields a median richness of nine.

TABLE 3
ICM DENSITY PROFILES

Model	a (kpc)	ρ (kg m^{-3})	ρa^β ($\text{kpc}^{1.9} \text{kg m}^{-3}$)	Environment	Reference
χ_1	10	1.7×10^{-23}	1.3×10^{-21}	Field & poor groups	Blundell et al. (1999); Garrington & Conway (1991)
χ_2	2	7.2×10^{-22}	2.7×10^{-21}	Field & poor groups	Kaiser et al. (1997); Canizares et al. (1987)
χ_3	391	7.2×10^{-26}	6.1×10^{-21}	Large groups & poor clusters	Jetha et al. (2007)
χ_4	30	5.0×10^{-23}	3.2×10^{-20}	Moderate clusters	Kaiser & Alexander (1999b); Jones & Forman (1984)
χ_5	260	5.9×10^{-24}	2.3×10^{-19}	Large clusters	Kaiser & Alexander (1999b); Jones & Forman (1984)

NOTE. — Density profiles given in terms of increasing density parameter, $a\rho^\beta$. The density and scale length are not independent parameters in the KDA model, but only appear in their combined form $a\rho^\beta$.

the median power of these distributions ($\sim 10^{38}$ W) and with a length typical for the jets in our sample (~ 100 kpc), the predicted radio luminosity is two orders of magnitude larger than the typical radio luminosity of the FR IIs in our sample.

As Bird et al. (2008) showed, lifetime estimates scale as the cube root of the median jet power. Nevertheless, an error in the power distribution by over an order of magnitude can produce errors in the lifetime calculations by a factor of at least three. To accurately determine the jet lifetime, we therefore need a reasonable estimate of the jet powers in our sample.

Since the KDA model is a one-to-one function of age and power to length and radio luminosity over the range of physically-motivated choices of the input and auxiliary parameters, it is possible to numerically invert it to produce an age and power given a length and luminosity. For any given jet in our sample, we compute the set of powers which reproduces the observed length over a range of ages from 10^6 yr to about 5×10^9 yr (at which point numerical calculations begin to stop converging⁴). This upper bound is well above numerous other constraints on the lifetime of AGN, and FR IIs specifically (e.g., Martini 2004; O’Dea et al. 2009). Because the observed projected length is only a lower bound on the true physical length of the FR II, we make an average correction of a factor of $4/\pi$ to the length to account for this projection effect. We similarly compute the set of powers which reproduces the observed luminosity over the same range of ages. The intersection of the loci of the two sets is then an estimate of the age and power of the FR II. Figure 5 illustrates the locus of constant length and the locus of constant luminosity for a typical FR II in our sample.

We perform this process for every jet in our sample with each of the five ICM models. The median powers and ages are presented in Table 4, and the distribution of the sample in power-age space for the Jetha et al. (2007) ICM density estimate is displayed in Figure 6. These median powers range from 4×10^{36} W to 10^{37} W, lower than the median jet power assumed in Bird et al. (2008) by over an order of magnitude. These jet powers are also lower than the minimum FR II jet power derived in Kaiser & Best (2007); we provide a plausible explanation for why their calculation is not inconsistent with our results in §3.2. Our results are consistent with other, simpler methods of estimating the jet power (e.g., Punsly 2005).

The resulting distribution of FR II jet powers in our sample is not well described by a truncated power law. To account for selection effects, we generate a set of mock catalogs (de-

TABLE 4
ESTIMATED MEDIAN JET POWERS AND AGES

ICM Density Model	A	Q_{med} (10^{35} W)	t (10^7 yr)
(1)	(2)	(3)	(4)
χ_1	2	211.3	9.8
χ_1	3	165.6	7.7
χ_1	4	145.0	6.6
χ_1	6	124.7	5.5
χ_1	8	113.9	4.8
χ_1	12	102.0	4.0
χ_1	16	95.1	3.5
χ_2	2	174.6	13.2
χ_2	3	134.6	10.4
χ_2	4	116.5	9.1
χ_2	6	99.0	7.3
χ_2	8	89.8	6.6
χ_2	12	79.7	5.4
χ_2	16	74.0	4.8
χ_3	2	142.9	18.5
χ_3	3	108.8	14.9
χ_3	4	93.3	12.8
χ_3	6	78.5	10.6
χ_3	8	70.7	9.3
χ_3	12	62.3	7.7
χ_3	16	57.5	6.9
χ_4	2	99.4	36.3
χ_4	3	75.0	29.1
χ_4	4	63.9	25.4
χ_4	6	53.1	20.8
χ_4	8	47.6	18.3
χ_4	12	41.6	15.2
χ_4	16	38.3	13.7
χ_5	2	68.4	79.2
χ_5	3	51.9	62.7
χ_5	4	44.5	54.6
χ_5	6	37.3	45.7
χ_5	8	33.6	39.7
χ_5	12	29.7	32.9
χ_5	16	27.5	29.2

NOTE. — The median powers and ages of the FR IIs in the full sample estimated using the method described in §3.3. Our default choice of density model and axial ratio is shown in bold. (1): The density model (defined in Table 3). (2): The axial ratio (defined in §4.2). (3): The estimated jet power. (4): The estimated current age. Due to selection effects there is no simple way to convert the median current age to a lifetime estimate.

⁴ Specifically, for sufficiently extreme parameters, Equation (A26) of Kaiser & Best (2007) fails to have a solution.

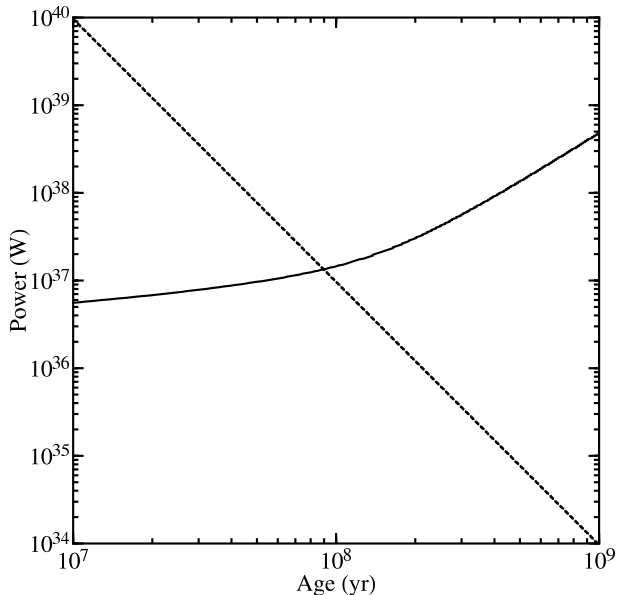


FIG. 5.— A graphical explanation of the procedure to find the age and power of an FR II source given its length and luminosity. The solid line is the locus of points in age-power space consistent with the jet’s observed luminosity, in this case $1.3 \times 10^{25} \text{ W Hz}^{-1}$. The dashed line is the locus of points consistent with the jet’s observed length, in this case 98.1 kpc. The intersection of the two lines is the only age and power consistent with the observed length and luminosity of the jet within the KDA model. The data shown in this plot are for a typical jet in our sample for an axial ratio of $A = 4$ and an ICM with $\rho = 7.2 \times 10^{-26} \text{ kg m}^{-3}$ and $a = 391 \text{ kpc}$. Because the observed length of an FR II is shorter than its true physical length due to projection effects, we make an average correction to the observed jet length before estimating its age and power.

scribed in further detail in §3.5) consisting of 10^6 FR IIs given random ages, redshifts, and orientations. If we assume that the jet powers are distributed as a truncated power law with a minimum power Q_{\min} and a slope α , a maximum likelihood analysis (described in further detail in §4.1, where it is applied to the length distribution and lifetime measurement) applied to the resulting power distributions indicates that the best fit is $Q_{\min} = 7.6 \times 10^{35} \text{ W}$, $\alpha = 2.2$ for the Jetha et al. (2007) ICM model and an axial ratio of 4. Although better fits exist in principle, the fraction of detectable FR IIs in them is so low that our sample size would be much less than 151 even if every BCG in the MaxBCG catalog hosted an FR II. Even in this best fit, a sample size of 151 FR IIs can only be recovered if $\sim 50\%$ of the BCGs in the MaxBCG catalog host FR IIs. We find that the power distribution is much better described by a log-normal distribution. A similar analysis shows that the best fit has a median power of $1.1 \times 10^{37} \text{ W}$ and a coefficient of variation of 2.2 under the same density and axial ratio assumptions. (We perform this fit for every choice of ICM density and axial ratio we examine in this work. See §4.2 and §4.3 for these choices.) A log-normal distribution not only fits the observed jet power distribution better than a power law, but it also does not require a very low detection probability, and hence does not require that a large fraction of BCGs harbor FR IIs ($\sim 2\%$ for a log-normal distribution vs. $\sim 60\%$ for a power law). The cumulative distribution of jet powers is presented in Figure 7 along with the best-fitting power law and log-normal distributions.

The true distribution is likely more complicated (and possibly an approximate power law) than log-normal, but only appears log-normal as a result of selection effects. Although the mock catalogs account for any biases due to our selection

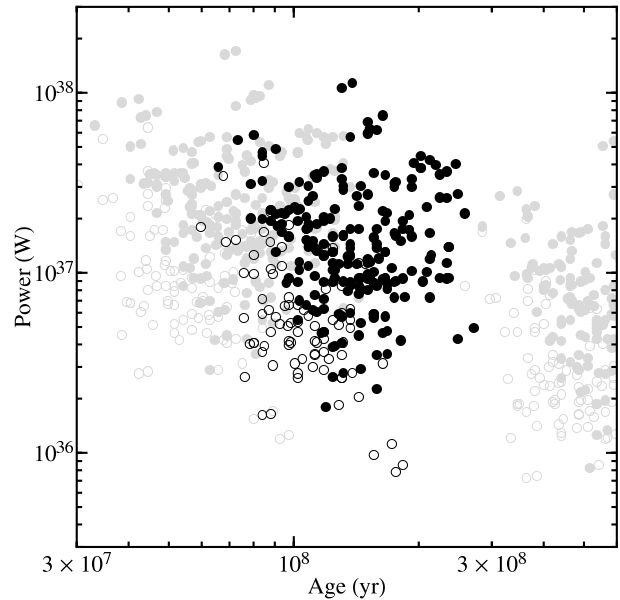


FIG. 6.— The distribution of the full sample (filled and open circles) and the volume-limited sample (filled circles only) in estimated jet power and age assuming an axial ratio of 4 and the χ_3 density model suitable for typical clusters (black points), the χ_1 density model suitable for galaxy groups (left group of light gray points), and the χ_5 density model suitable for the richest clusters (right group of light gray points). (See Table 3 for definitions of the density models.) Because the age and power estimates indicated here are determined simultaneously, errors in the power estimate can induce errors in the age estimate, and vice versa. Furthermore, although an average correction is made for projection effects, the age and power estimates in this figure do not reflect any distribution in projection angle. The age estimates in this figure are therefore only approximate. We use the length distribution to constrain the age more precisely because it is more strongly dependent on age than luminosity. Because the uncertainty in our estimates is dominated by systematic uncertainties in the ICM density and axial ratios of the FR IIs, we do not show error bars in this plot. Systematic uncertainties are on the order of a factor of two in both age and jet power based on variation in these estimates over a reasonable range of ICM densities and axial ratios.

algorithm, they do not account for selection effects imposed by the MaxBCG catalog. Specifically, the distribution of BCG stellar luminosities in the MaxBCG catalog can be much better described by a log-normal distribution than a power law. Since BCG stellar luminosities are correlated with FR II jet powers (as we show in §5.1.1), it is not surprising that our observed distribution of jet powers resembles a log-normal distribution. The log-normal distribution in BCG luminosities may be the result of the steep galaxy luminosity function at high luminosities and the minimum richness cutoff of the sample. A study of jet powers in lower-luminosity galaxies and field galaxies could determine if the intrinsic jet power distribution is log-normal for all galaxies.

While the method described in this section produces estimates of the ages of the FR IIs, we do not expect them to be particularly precise. This is because the estimates of the lengths and ages of the FR IIs place equal weight on the equation for luminosity evolution and the equation for length evolution. The length evolution of the FR II is relatively straightforward to model, because it only relies on dimensional analysis, and hence is consistent across many models. The luminosity evolution, on the other hand, is much more difficult to model and so has greater uncertainty. Even if the equation for luminosity evolution were known perfectly, there is also a greater uncertainty in the flux measurement than in the length measurement. This is because the sources are extended and therefore flux from diffuse components can be lost and flux from spatially coincident sources can be added. We therefore

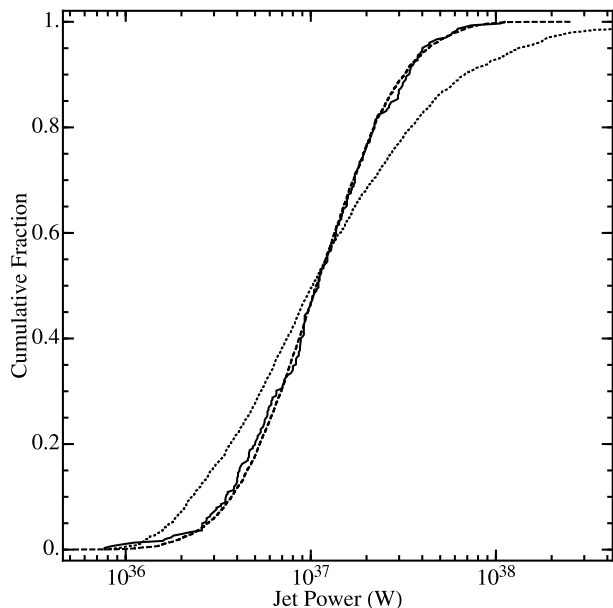


FIG. 7.— The cumulative distribution of jet power for FR IIs in our sample (solid line), the best-fitting power law distribution (dotted line), and the best-fitting log-normal distribution (dashed line). These distributions are the observed distributions from mock catalogs which take selection effects into account to make them directly comparable to the observed sample. The power law distribution shown here makes the implausible requirement that $\sim 60\%$ of BCGs in the MaxBCG harbor FR IIs, but only $\sim 7\%$ are detected. Although better-fitting power law distributions exist, they require even smaller detection fractions; even if all BCGs in the MaxBCG catalog harbored FR IIs, these distributions predict FR II sample sizes much less than the 151 we observe. The log-normal distribution, by contrast, predicts a detection fraction of $\sim 60\%$.

only use this process to estimate the jet power to within a factor of a few and then use more precise methods to measure the lifetime. Because the lifetime calculation depends only on the cube root of the jet power, the uncertainty in the power estimate will not introduce an error in the lifetime calculation of more than a factor of two.

3.4. The $Q-P_{1.4}$ Relation

Several authors have sought a simple power-law relationship between the jet power and radio luminosity (Willott et al. 1999; Punsly 2005; Bîrzan et al. 2008; Cavagnolo et al. 2010). Although the jet power is the fundamental physical parameter of interest in radio galaxies, it is not easily measurable. A simple, approximate conversion between jet power and the observed radio luminosity would be useful to estimate jet powers in large samples of radio galaxies.

We fit the powers estimated in §3.3 to a power-law in 1.4 GHz radio luminosity. For the Jetha et al. (2007) ICM density model and an axial ratio of 4, we find the best fit to be

$$\log Q = 0.95(\pm 0.03)\log P_{1.4} + 13.4(\pm 1.1) \quad (7)$$

where both Q and $P_{1.4}$ are in Watts and the quoted errors are purely statistical. Variation of the ICM density and axial ratio changes the normalization, but leaves the exponent of the power law unchanged to within the quoted error. This fit is shown in Figure 8. The scatter in this relation is largely due to the fact that variations in length (and hence age) are ignored.

This relation is steeper than the relations found by Bîrzan et al. (2008) and Cavagnolo et al. (2010), who find exponents of 0.35 ± 0.07 and 0.75 ± 0.14 , respectively. Our relation is, however, consistent with the relation between Q and the radio luminosity at 151 MHz derived by Willott et al. (1999) and Punsly (2005), who found an exponent of 0.86.

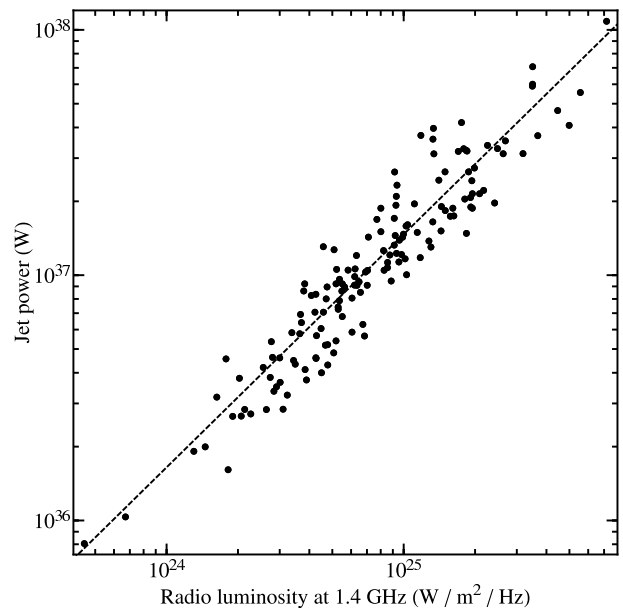


FIG. 8.— The best-fit power law relation between radio luminosity at 1.4 GHz and the jet power assuming the χ_3 density model (defined in Table 3) and an axial ratio of 4. Changes to the ICM density and axial ratio change the overall normalization but do not have a large effect on the exponent. The method for calculating the jet powers is described in §3.3. We emphasize that the best fit relation is heavily model-dependent due to our use of the KDA model to convert from jet length and radio luminosity to the jet power. This relation is therefore best interpreted more as a prediction of the KDA model than a direct measurement of the $Q-P_{1.4}$ relation.

We emphasize that our fit is heavily model-dependent because our conversion from jet length and radio luminosity to jet power is derived from the KDA model. While the KDA model likely provides estimates of jet powers which are correct to within a factor of a few, any errors in the relationship between jet power and radio luminosity derived in the model will be reflected in the exponent of our fit. The scatter in this relationship will also be influenced by the intrinsic jet power and age distribution of the sample. The scatter for our sample may be relatively modest because the jet power distribution follows a log-normal distribution, which may not be the case for all FR II samples due to the selection of the input cluster catalog (see §2.1).

3.5. Mock Catalog Generation

We compare the observed length distribution of FR IIs to mock catalogs to infer their intrinsic properties. These mock catalogs are based on large, simulated datasets that sample a suite of KDA model parameters (e.g., the ICM density and axial ratio) and a range of maximum ages. For any given choice of KDA model parameters, we create 31 mock catalogs with maximum ages ranging from 1.1×10^7 to 1.2×10^9 yr and distributed evenly logarithmically. Roughly 1.3×10^6 jets are then created by randomly choosing an age, power, and redshift for each jet. The age is sampled from a uniform distribution ranging from 0 to the maximum age chosen for that particular catalog and the jet power is sampled from the log-normal distribution derived in §3.3. To account for selection effects, we decrease the median power by 15%, an empirically determined amount for which the jet power distribution of the mock catalogs best matches the observed jet power distribution. The redshift of the simulated jet is then sampled from the redshift distribution of the entire MaxBCG catalog. (The redshift distribution is necessary when calculating the jet luminosities due to the effect of the CMB energy density on

synchrotron losses.) We assume that the birth rate of FR IIs is constant across the redshift range of the MaxBCG catalog. The support for this assumption is discussed in §5.3.

Once a jet has been created, we calculate its K -corrected luminosity and randomly orient it on the sky to calculate its projected length. We then apply the selection criteria described in §2.3 to create a mock catalog for that parameter set.

4. THE FR II LIFETIME

4.1. Maximum Likelihood Fitting

Our approach to estimate the maximum lifetime for FR IIs is to compare the projected length distribution of the mock catalogs to the observed distribution. We fit the observed distribution to the mock catalogs with the maximum likelihood method. The result is the best-fit maximum age for a given set of model parameters.

The likelihood of any maximum age is determined by constructing a probability distribution function (PDF) of the length distribution for a mock catalog with 1-kpc-wide bins. If the number of jets in the mock catalog that fall into the i^{th} bin is n_i , the probability that a jet will fall in that bin is n_i/N , where N is the total number of jets in the mock catalog, $\sum_i n_i$. With a PDF, f , so defined, the likelihood of any model is then

$$\mathcal{L} = \prod_j f(l_j), \quad (8)$$

where l_j is the projected length of the j^{th} jet in the observed sample. For any given choice of parameters, we take the best-fit lifetime to be the maximum age of the mock catalog which maximizes the likelihood. The error on the lifetime calculation is taken to be the FWHM of the likelihood distribution.

Figure 9 shows likelihood distributions for several models. The length distribution of the mock catalog for a sample model at three ages is displayed with the observed length distribution in Figure 10. Because the projected length distribution is extremely sensitive to age, we can determine the FR II lifetime with relatively high precision. Table 5 presents the lifetimes and their uncertainties for every model used. We note that we only measure the *typical* FR II lifetime and there is likely some intrinsic dispersion which is larger than the statistical uncertainties indicate. We discuss any correlations between the typical FR II lifetime and various jet properties in §5.1.4. The best-fitting lifetime for our default ICM model is 1.9×10^8 yr.

4.2. Dependence on Axial Ratio

We define the axial ratio as the ratio of the length of the lobe to the perpendicular distance between the edge of the lobe and its axis. (Some other studies define the axial ratio as the ratio between the length of the lobe and the width of the lobe; our definition is twice this other convention.) Due to projection effects, background noise, and the fact that the shapes of real radio lobes are more complicated than the simple geometry of radio lobe models, unbiased and robust measurements of the axial ratios of FR II sources are difficult to obtain. Nevertheless, nearly all estimates fall between 2 and 16 (Leahy & Williams 1984; Machalski et al. 2004). Some studies of extremely powerful jets have found even larger axial ratios, but there appears to be a relationship between jet power and axial ratio, with more powerful jets having unusually large axial ratios (Leahy et al. 1989). While it is possible to estimate the axial ratios of the FR IIs in our sample from the FIRST images, the width of the lobes are in many cases comparable to the size of the FIRST PSF, so such estimates only

TABLE 5
FR II LIFETIMES & STATISTICAL ERRORS

ICM Density Model	A	t_{lifetime} (10^7 yr)
(1)	(2)	(3)
χ_1	2	15.5 $^{+0.3}_{-0.8}$
χ_1	3	11.9 $^{+0.4}_{-0.2}$
χ_1	4	10.0 ± 0.2
χ_1	6	8.3 ± 0.2
χ_1	8	7.1 ± 0.2
χ_1	12	6.0 ± 0.4
χ_1	16	5.2 ± 0.1
χ_2	2	20.3 ± 0.4
χ_2	3	16.2 $^{+0.6}_{-0.3}$
χ_2	4	14.1 $^{+0.8}_{-0.5}$
χ_2	6	11.7 ± 0.2
χ_2	8	9.9 ± 0.2
χ_2	12	8.0 ± 0.2
χ_2	16	6.9 ± 0.4
χ_3	2	28.1 $^{+0.2}_{-0.1}$
χ_3	3	23.2 ± 0.4
χ_3	4	19.2± 0.4
χ_3	6	16.2 ± 0.3
χ_3	8	14.4 ± 0.5
χ_3	12	11.7 $^{+0.3}_{-0.5}$
χ_3	16	10.2 ± 0.4
χ_4	2	55.9 ± 0.9
χ_4	3	45.3 ± 1.8
χ_4	4	38.1 $^{+1.5}_{-0.7}$
χ_4	6	31.5 $^{+1.8}_{-1.2}$
χ_4	8	27.6 $^{+1.0}_{-0.6}$
χ_4	12	23.6 $^{+0.5}_{-0.3}$
χ_4	16	19.9 $^{+0.8}_{-0.3}$
χ_5	2	122 ± 3
χ_5	3	105 $^{+2}_{-4}$
χ_5	4	84.9 ± 1.7
χ_5	6	68.9 ± 2.6
χ_5	8	59.1 $^{+2.4}_{-1.2}$
χ_5	12	50.8 $^{+0.9}_{-2.9}$
χ_5	16	42.8 $^{+1.6}_{-0.8}$

NOTE. — FR II lifetimes with the maximum likelihood for every density model and axial ratio. The default choice of density and axial ratio is in bold. (1): ICM density model (defined in Table 3). (2): Axial ratio (defined in §4.2). (3): FR II lifetime. The quoted uncertainties are purely statistical and are derived from the FWHM of the likelihood distribution.

provide lower bounds on the axial ratios. Since our sample does not include atypically powerful jets, we simply examine axial ratios within the entire plausible range of $2 \leq A \leq 16$ and note that our estimates are most consistent with an axial ratio of 3 – 4, but could be larger. Higher-resolution data of some of the FR IIs in our sample would be needed to accurately measure their axial ratios.

To first order, one expects that as the axial ratio increases, the lifetime should decrease. At high axial ratios, the jet does not need to expend as much energy inflating a fat cocoon around it and can therefore drill through the ICM more efficiently; thus, a jet of given power with a large axial ratio can reach the same length as a jet with a small axial ratio in less time. But this simple relationship is complicated by the fact that the axial ratio changes the estimated power as well. A

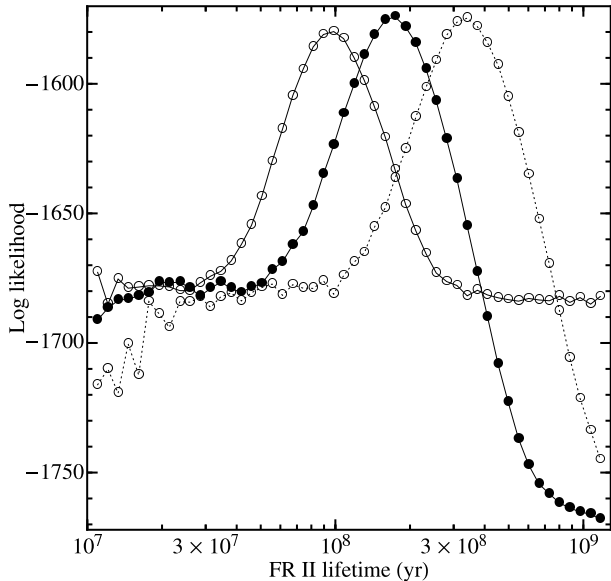


FIG. 9.— Likelihood distributions of three models for a range of FR II lifetimes. The peak of the likelihood distribution for a particular model is the lifetime that best matches the observed data. The solid points represent the likelihood distribution for the default ICM density model χ_3 and an axial ratio of 4. The open circles connected by a solid line represent the default ICM density model χ_3 and an axial ratio of 12. The open circles connected by a dotted line represent the χ_4 ICM density model and an axial ratio of 4. See Table 3 for a description of the ICM density models.

jet with a larger axial ratio requires less power to produce a given length in a given time, so larger axial ratios will lead to lower power estimates. This will partially counterbalance the increased age estimate and produce a smaller axial ratio dependence on age than one would naively expect from the jet length and age alone. Nevertheless, because the lifetime is relatively insensitive to the power, this correction does not dominate.

Bird et al. (2008) found that the axial ratio has a stronger effect on FR II lifetime calculations than all other KDA model parameters. To evaluate the dependence of our FR II lifetime measurements on axial ratio, we calculated the lifetimes of jets in our sample for different axial ratios. For any particular choice of axial ratio, we used the KDA model to estimate the jet powers, generated a set of mock catalogs across a range of ages, and fit these to the observed length distribution with the maximum likelihood method described in §4.1. The dependences of power and lifetime measurements on the assumed axial ratio are shown in Figures 11 and 12. The inferred power decreases as the axial ratio increases, but the effect is only approximately a factor of two decrease over a factor of eight increase in axial ratio. The age estimate similarly decreases as the axial ratio increases, with the effect also being a roughly factor of two decrease over a factor of eight increase in axial ratio. This effect is even weaker when the change in inferred jet power is taken into account.

4.3. Dependence on the ICM Model

The model length distribution also depends on the ICM density parameter. ICM density measurements of group and cluster samples can vary by several orders of magnitude (Vikhlinin et al. 2006; Jetha et al. 2007; Freeland & Wilcots 2011). Since the density of the model ICM can potentially have a large effect on FR II lifetime estimates, we produced sets of mock catalogs spanning about two orders of magnitude in density. The density profiles we use and their references are

listed in Table 3.

At higher densities, a jet of a given power will require more time to grow to a given length, so to first order, increased densities will lead to increased lifetime estimates, approximately linearly. However, increased densities also increase the luminosity of a jet at a fixed power; hence higher densities lead to lower power estimates. This, in turn, will result in yet longer lifetime estimates in second order.

For each ICM model, the length distribution of the mock catalogs was fit to the observed length distribution of the flux-limited sample with the maximum likelihood method described in §4.1. The dependence of power and lifetime measurements on the assumed ICM model are shown in Figures 13 and 14. These figures indicate that larger densities yield larger lifetime estimates and smaller power estimates, though in the case of the jet power estimates the dependence appears to be more complicated in detail than a power law.

4.4. The FR II Duty Cycle

Because our mock catalogs take into account the biases induced by selection effects on our sample, we use them to calculate a robust upper bound on the duty cycle of FR IIs in BCGs, where the FR II duty cycle is the average FR II lifetime divided by the fraction of time that the jet remains active. Although it is not possible to directly measure the fraction of time that a jet remains active, a lower limit on this fraction can be found in a straightforward manner. If we assume that every BCG in a cluster has a radio jet at some point in its life, then the fraction of time that a jet is active is the number of BCGs with radio jets divided by the total number of BCGs. Since it might be that many BCGs never have a radio jet, this fraction is necessarily a lower limit.

The total number of BCGs in our sample is 13,823, the size of the MaxBCG catalog of Koester et al. (2007a). The number of BCGs with FR IIs is our sample size of 151 FR IIs plus some additional FR IIs that fall below our selection criteria. To estimate the number of FR IIs that are missed, we calculate the fraction of simulated jets that pass all of the detection thresholds in our mock catalogs. The mock catalogs are populated with jets resembling the underlying population of FR IIs, so the fraction of jets which pass our detection cuts is an estimate of the completeness of our sample. For the best-fit age and the default parameters, this completeness fraction is 61.7%. The overwhelming majority of missed sources are too short. We divide the number of jets in our sample by this completeness fraction and estimate that there are approximately 245 FR IIs in these BCGs. The fraction of time that a jet is active is then $245/13,823$, or 1.8%. This fraction is in agreement with the value found by Bird et al. (2008) for galaxies in the group environment. Combined with our best estimate of the FR II lifetime of 1.6×10^8 yr, this yields an upper bound for the duty cycle of 9×10^9 yr. As this upper bound is comparable to a Hubble time, it implies that most BCGs undergo an FR II phase only once. If a substantial fraction of BCGs are never FR IIs (either being always inactive or only appearing as FR Is), then FR IIs could be episodic.

5. THE RELATIONSHIP BETWEEN FR IIS AND THEIR ENVIRONMENTS

We here determine whether any of the properties of FR IIs determined in the above analysis are correlated with the FR II environment. In §5.1 we examine correlations of jet power with stellar luminosity, BCG velocity dispersion, cluster richness, and FR II lifetime. The impact of our assumptions about

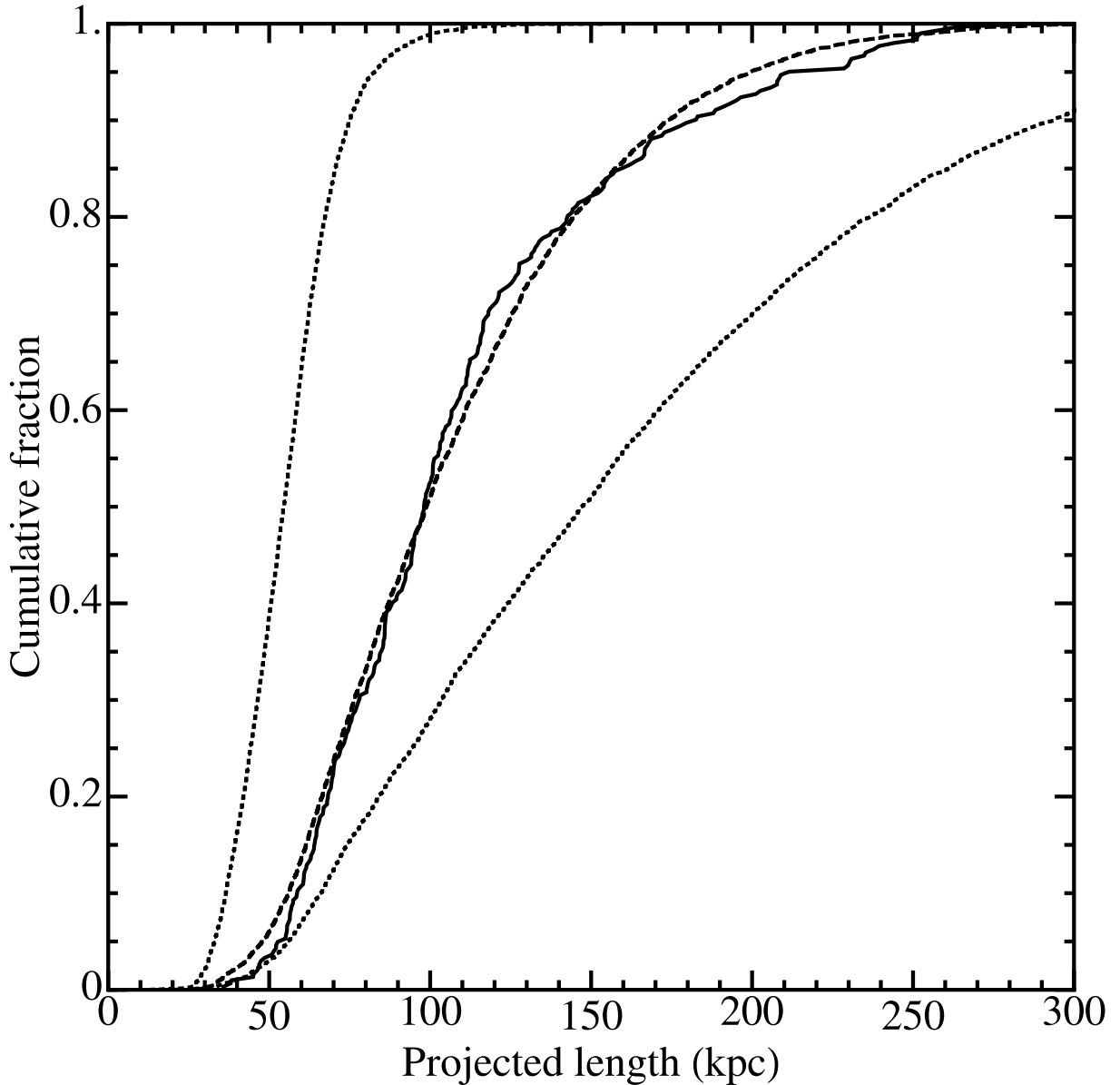


FIG. 10.— A comparison of the cumulative projected length distribution of the sample (solid line) to the cumulative length distributions of a model for three different lifetimes (dashed and dotted lines) assuming the default ICM density χ_3 (see Table 3) and an axial ratio of 4. The dashed line shows the FR II lifetime from the model with the maximum likelihood, which in this case was 1.9×10^8 yr. The left and right dotted lines represent FR II lifetimes of 6.1×10^7 yr and 3.4×10^8 yr, respectively.

the ICM model used in §5.1 is assessed in §5.2. We finally examine the broader relationship between the FR II and radio galaxy fractions and galaxy cluster richness in §5.3.

5.1. Correlations with Jet Power

Radio jets are powered by the accretion of gas onto nuclear, supermassive black holes (SMBHs). Although the mechanism by which infalling gas is expelled and collimated from the SMBH is not well understood, most jet models rely on some variant of the Blandford-Znajak (BZ) mechanism (Blandford & Znajek 1977). The BZ mechanism explains jet outflows from SMBHs by postulating a magnetic field anchored to an accretion disc around a rapidly spinning SMBH. As the accretion disk rotates around the SMBH, the field lines become wound around the spin axis. Some charged particles falling into the SMBH will then follow the field lines and escape along the spin axis of the SMBH. Jet models which apply the BZ mechanism find that the power that can be extracted

from the SMBH and injected into the jet is roughly proportional to the accretion rate and the square of the SMBH spin (McNamara et al. 2011). Larger black holes should therefore generally produce more powerful jets. It is interesting to see whether we can recover this relationship in our FR II sample. While direct measurements of SMBH masses are not available at the distances in our sample, we can check for the existence of a correlation between jet power and two proxies for SMBH mass: BCG luminosity and BCG velocity dispersion. We also search for a correlation between jet power and cluster richness, which may be related to the fuel source and thus the accretion rate, and between lifetime and cluster properties.

Because the MaxBCG catalog is not complete and our FR II sample is flux-limited, selection effects could induce an artificial correlation between jet power and BCG or cluster properties. For instance, if the MaxBCG catalog suffered from Malmquist bias, a distant FR II in our sample would have to be both luminous at radio wavelengths (and hence have a large

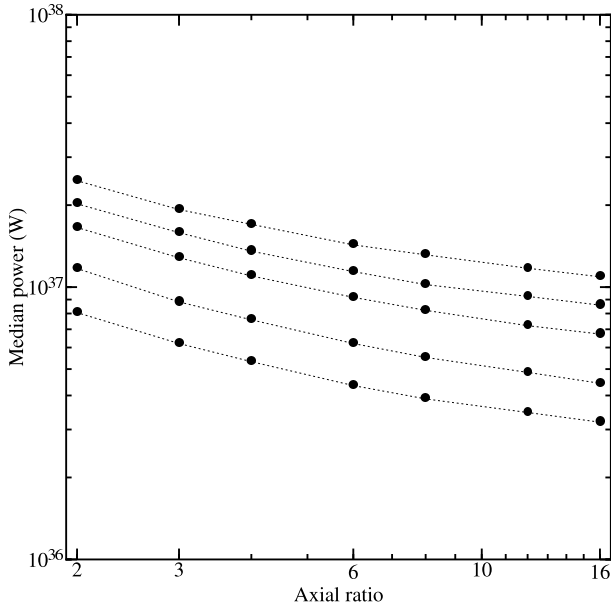


FIG. 11.— The dependence of the axial ratio on the median inferred power of the FR II sample. The points along each dotted line represent the median powers inferred for a particular density model. From bottom to top, the density models used are $\chi_1 - \chi_5$. See Table 3 for the details of each density model.

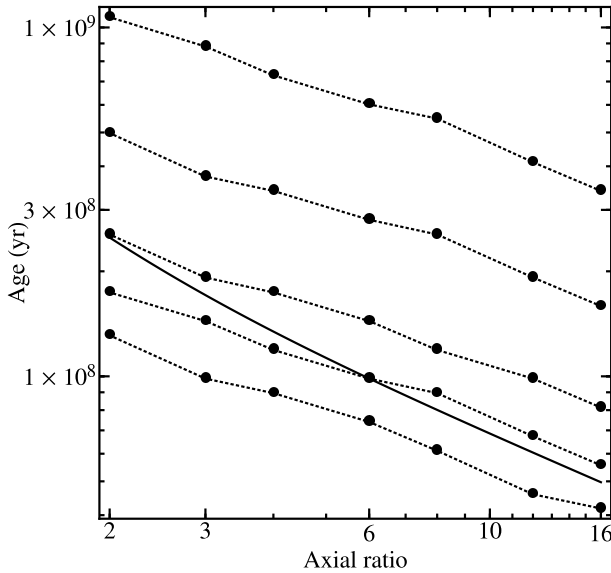


FIG. 12.— The dependence of FR II lifetime estimates on the assumed axial ratio. Each dotted line represents a set of lifetime estimates for a single density. Lower tracks assume lower densities. The densities used are listed in Table 3. The solid line represents the axial ratio dependence one would expect if one only considered the effect of axial ratio on the length of the jets as a function of time. Because the axial ratio also has an effect on our power estimates of the jet which tends to counteract the effect of axial ratio on length evolution, the final lifetime estimate is less sensitive to the axial ratio than found by other studies (e.g., Bird et al. 2008).

jet power) and be hosted by a luminous galaxy. This would lead to a concentration of FR IIs with high jet power and high BCG optical luminosity in the sample and thereby induce a correlation between the two properties. Completeness tests based on mock catalogs indicate that the MaxBCG catalog is principally biased against low-mass clusters since the member galaxies of such clusters tend to be less significant overdensities, although there is a slight bias against extremely high-mass clusters as well (see Figure 7 of Koester et al. 2007a, for the detailed completeness function of the MaxBCG catalog).

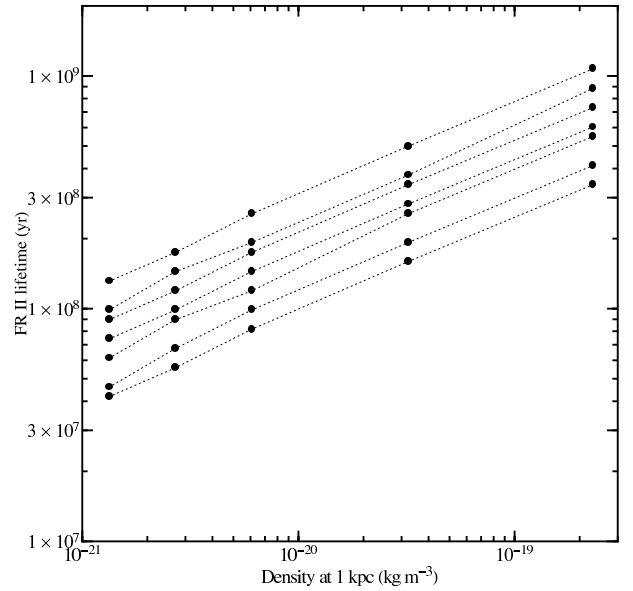


FIG. 13.— The dependence of the FR II lifetime calculation on the density of the ICM. In each case the density profile is described by a power law with a slope of 1.9. Each track represents a different choice of axial ratio; lower tracks have larger axial ratios. The values of the axial ratios are the values of the points in Figures 11 and 12.

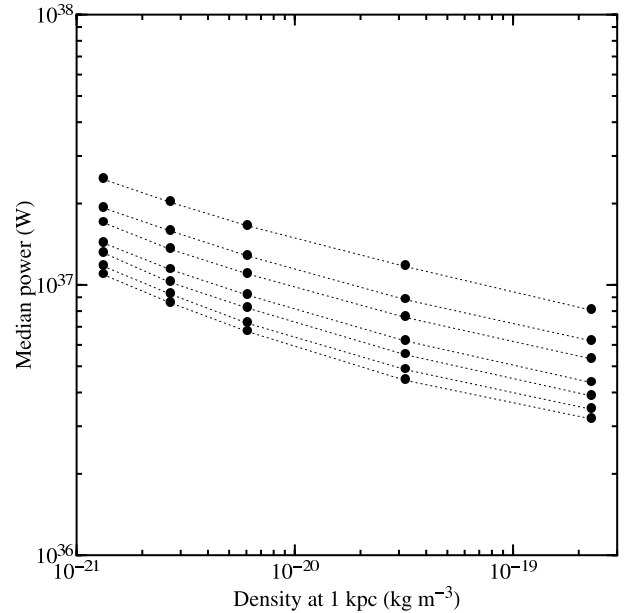


FIG. 14.— The dependence of the estimated FR II jet power on the density of the ICM. Each track represents a different choice of axial ratio; lower tracks have larger axial ratios. Refer to Figures 11 and 12 for the axial ratio of each track.

Low-mass clusters typically host lower-luminosity BCGs, so we should expect some correlation between jet power and BCG luminosity due to these selection effects. To avoid this bias, we use the volume-limited sample described in §2.4 to search for correlations between measured properties of the FR IIs and properties of their hosts. We note that while we do not remove the selection biases of the MaxBCG catalog, selection biases must be present in both variables to induce a correlation; mitigating the selection biases in just one variable is sufficient to remove this correlation.

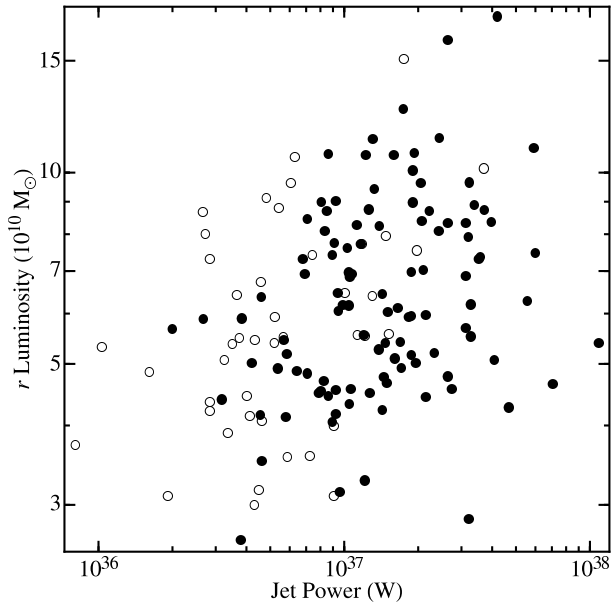


FIG. 15.— The correlation between the r -band luminosity of the host BCG and the estimated jet power. Filled circles represent jets in the volume-limited sample (see §2.4) and open circles represent jets in the full sample, but not the volume-limited sample. The correlation between the r -band luminosity and the jet power for jets in the volume-limited sample is 0.284; there is a 0.3% chance that this correlation could be drawn from an uncorrelated population. When the jets from the full sample are included, the correlation becomes stronger and more statistically significant.

5.1.1. The Correlation between Jet Power and Stellar Luminosity

The MaxBCG catalog provides a K -corrected r -band and i -band luminosity for every BCG in the sample. Because elliptical galaxies generally exhibit very little star formation and have little dust, both the r - and i -band luminosities should be well-correlated with the stellar mass, which is correlated with the SMBH mass (Novak et al. 2006 and references therein). If there is some power-law relationship between BCG luminosity and SMBH mass, we expect a correlation between the logarithm of the BCG luminosity and the logarithm of the jet power. We calculate that the Pearson correlation coefficient (Pearson 1895) between $\log Q$ and $\log L_r$ is 0.284. Given that our volume-limited sample has 106 degrees of freedom, the probability that a correlation coefficient of 0.284 or higher could be randomly drawn from uncorrelated data is only 0.3% and therefore statistically significant. A correlation of similar strength exists between the i -band luminosity and jet power. Since jet power is very strongly correlated to radio luminosity (see §3.3), a correlation of similar statistical significance exists between the radio luminosity of the radio lobes and the optical luminosity of the host galaxy. We show the relationship between jet power and r -band luminosity in Figure 15.

5.1.2. The Correlation between Jet Power and BCG Velocity Dispersion

The velocity dispersions of elliptical galaxies are tightly correlated with their nuclear SMBH masses (e.g., Gültekin et al. 2009). If there is a correlation between jet power and SMBH mass, we also expect a correlation between jet power and host velocity dispersion. We calculate the Pearson correlation coefficient between $\log Q$ and $\log \sigma$ and find it to be only 0.116. There is a 33% chance that this correlation could be drawn from an uncorrelated population, and is therefore not statistically significant. This result is at odds with

the correlation between jet power and BCG stellar luminosity and may be due to two reasons. First, SDSS does not have spectra of the BCGs of all of the FR IIs in our sample. We only have velocity dispersions for two-thirds of the BCGs in the volume-limited sample, which reduces the statistical power of our sample. Second, and likely more important, is that although the stellar luminosities of elliptical galaxies are strongly correlated with their velocity dispersions, velocity dispersion is a weak function of luminosity (proportional to the fourth root of luminosity; Faber & Jackson 1976). Our FR II sample has a dynamic range in BCG luminosity of roughly an order of magnitude. Even if jet power and optical luminosity were perfectly correlated, the resulting correlation between jet power and velocity dispersion would exhibit a dynamic range of less than a factor of 2. This is small enough to be overwhelmed by moderate scatter.

5.1.3. The Correlation between Jet Power and Cluster Richness

Richer clusters tend to host larger BCGs that, in turn, tend to host larger SMBHs. Richer clusters also have more hot gas and many clusters have cooling times shorter than 1 Gyr. With larger SMBHs and a larger reservoir of accretion material, it is plausible that cluster richness would be correlated with jet power. Alternatively, such a correlation could be present due to a correlation between jet power and BCG luminosity paired with a correlation between BCG luminosity and cluster richness. We calculate that the Pearson correlation coefficient between $\log Q$ and $\log N_{\text{gal}}$ is 0.094. There is a 33% probability that this correlation could be drawn from an uncorrelated population and therefore it is not statistically significant. The non-detection is not too surprising as we expect that this correlation would be weak at best since cluster richness is a global property of the cluster and the jet power depends on the microphysics governing the immediate vicinity of the SMBH.

5.1.4. Correlations with FR II Lifetime

The FR II lifetime is indicative of the length of time that a galaxy can successfully supply its SMBH with cold gas. Since the mechanism that supplies this gas is not well understood, we use our data to determine if FR II lifetime is correlated with any BCG or cluster properties. We test for a correlation in two different ways. The first method is identical to the method for measuring correlations with BCG and cluster properties explained above. When we estimate the FR II jet power (described in §3.3), we simultaneously estimate a crude (due to projection effects) FR II age for every jet in our sample. We then calculate the Pearson correlation coefficient between these nominal ages and various BCG and cluster properties (such as the BCG stellar luminosity). We find that none of the correlations between age and the BCG and cluster properties discussed above are statistically significant. The major drawback of this method is that the age estimate is sensitive to the length of the FR II and, due to projection effects, the measured projected length can be substantially smaller than the lobe length. While we make average corrections for projection effects, they nevertheless introduce scatter into the relationship between the FR II age and the various BCG and cluster properties. Furthermore, any individual FR II is almost equally likely to be detected at any point in its lifetime. Since we use the FR II's estimated age (not its lifetime), this will also introduce significant scatter.

Our second approach is to split the sample into two bins at the median of each parameter and test for correlations. This

provides two length distributions for each parameter. We perform the maximum likelihood analysis described in §4.1 and fit these distributions to the length distributions of the mock catalogs and see if there is a statistically significant difference in lifetimes between FR IIs in the two bins. However, we find no difference in lifetime between the two bins when we split by stellar luminosity, BCG velocity dispersion, or cluster richness.

5.2. The Impact of the ICM

The above analyses were all performed under the straightforward but unrealistic assumption that the ICM is identical for all clusters in our sample. It is known, however, that richer clusters tend to harbor denser ICMs with larger scale radii. We therefore split our sample into two bins at the median richness (14) to reexamine how strongly the FR II jet power and lifetime relate to the host cluster ICM. The low richness bin has richness values from 10 to 14. We assign these clusters the intermediate ICM model (χ_3 in Table 3) from Jetha et al. (2007), which is derived from large groups and small clusters with a median richness of nine. Richer clusters (greater than 14) are assigned the densest model (χ_5 in Table 3), which is the geometric mean of the densities found by Jones & Forman (1984) for clusters with a median richness of 20.

For each FR II we estimate the jet power with the method described in §3.3 and the density appropriate to the richness of the cluster. The power distribution as a function of richness is shown in Figure 16. Although there is a correlation between richness and FR II jet power that is statistically significant at the two-sigma level, it is weak. If we simply compare the mean power of all jets less than or equal to the median richness with those greater than the median richness, we find that the jets in richer clusters are, on average, less powerful by a factor of 2. Although this density parameterization is somewhat artificial because the ICM density is expected to steadily continue to increase with richness, albeit with substantial scatter, and spans an extreme range in density, this parameterization should be sufficient to identify a strong correlation. As the correlation between inferred jet power and cluster richness is only marginal, both this result and those in §5.1 imply that the properties of FR IIs are relatively insensitive to large-scale environmental factors.

5.3. FR II and Radio Galaxy Fraction vs. Cluster Richness

If radio-mode feedback can prevent substantial gas cooling in clusters, there may be an increase in duty cycle, lifetime, and jet power with cluster richness. In the previous subsections, we showed there is no strong correlation between jet power or lifetime and richness. Here we investigate differences in duty cycle with the fraction of clusters with an FR II source and the fraction of clusters with a radio source of any kind. We calculate the FR II fraction in richness bins that have been corrected for undetected sources. This process would eliminate any potential spurious correlations between FR II fraction and cluster richness due to the correlation between cluster richness and redshift.

To calculate the fraction of all radio sources we cross-correlated the FIRST and MaxBCG catalogs. Rather than select radio sources at least $10''8$ (two FIRST resolution elements) from the BCG as for FR IIs, we selected BCGs with a radio source within $10''8$. To mitigate Malmquist bias, we furthermore selected only those radio sources whose radio luminosity was greater than $1.7 \times 10^{22} \text{ W Hz}^{-1}$ at 1.4 GHz.

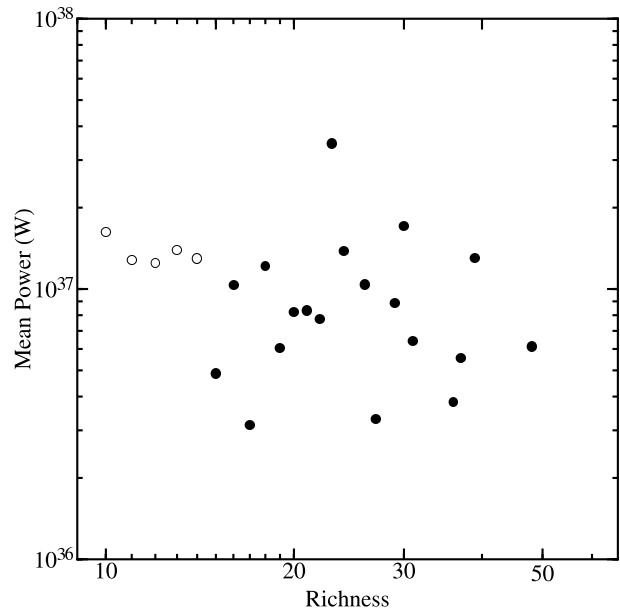


FIG. 16.— The FR II mean jet power as a function of host cluster richness after applying a parameterization between cluster richness and ICM density. Since larger clusters tend to have denser ICMs, we split our sample along the median cluster richness of 14 and assume the χ_3 ICM model (see Table 3) from Jetha et al. (2007) for the low-richness clusters (open circles) and the χ_5 ICM model from Jones & Forman (1984) for the high-richness clusters (filled circles). We then estimate the jet power of each FR II with the inferred density as described in §3.3. The resulting correlation between jet power and cluster richness, while statistically significant, is weak.

This corresponds to the lowest luminosity that FIRST can detect at $z = 0.3$, the largest redshift in the MaxBCG catalog. Bird et al. (2008) performed a similar analysis using two additional, more stringent luminosity cutoffs and found no substantive difference in the relationship between radio fraction and cluster richness or luminosity. We therefore only use this luminosity cutoff.

The FR II and radio fractions as a function of cluster richness are shown in Figure 17. There is an increase in radio fraction by a factor of 1.5 – 2 with richness. Although the statistics on the FR II fraction are weaker due to its smaller sample size, there appears to be a corresponding trend in FR II fraction with cluster richness. We perform a similar analysis to examine the relationship between the FR II and radio fractions with BCG luminosity and find that both fractions increase strongly with BCG luminosity. These relationships are shown in Figure 18. The increase in the radio fraction with stellar luminosity is similar to the increase in the radio fraction with stellar mass shown by Best et al. (2007) and ?. We also find that the FR II fraction does not evolve over the range of redshifts in the MaxBCG catalog. We show the FR II fraction across the redshift range of the volume-limited sample in Figure 19.

6. DISCUSSION

6.1. Comparison to FR II Lifetime Measurements in the Literature

Our measurement of the FR II lifetime is most directly comparable to the FR II lifetime measurement by Bird et al. (2008) as their approach is largely identical to our own. They also modeled the observed FR II length distribution with mock catalogs to account for selection and projection effects and used the KDA model to determine the length and luminosity evolution. Bird et al. (2008) found an FR II lifetime of 1.5×10^7 yr, which is an order of magnitude below our

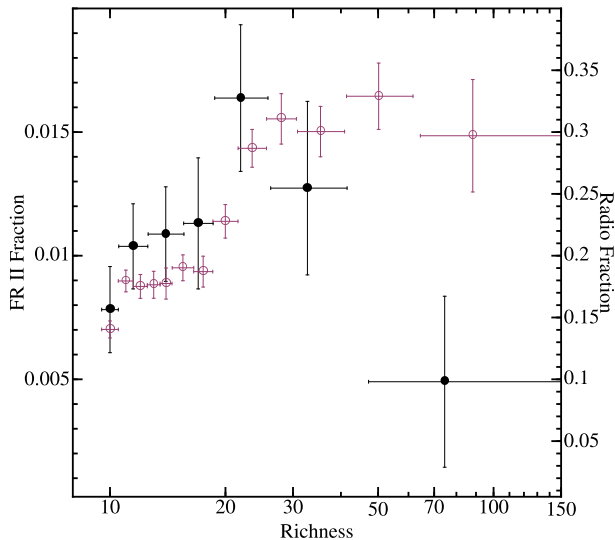


FIG. 17.— The FR II fraction (filled circles) and fraction of all radio sources (open circles) as a function of cluster richness in the MaxBCG catalog. We define radio sources to be BCGs with radio emission detected by FIRST within $10''/8$ (i.e. two FIRST resolution elements). The horizontal error bars are the bin widths and the vertical error bars are the binomial errors.

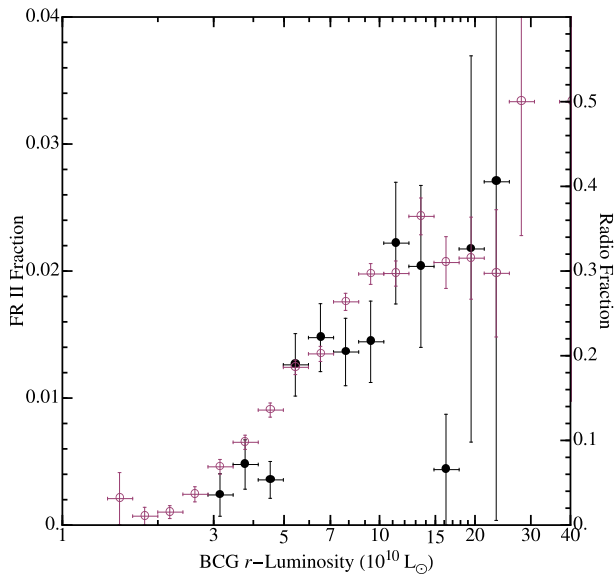


FIG. 18.— The FR II fraction (filled circles) and radio fraction (open circles) as a function of the BCG r -band luminosity. Radio sources are defined as in Figure 17. The horizontal error bars are the bin widths and the vertical error bars are the binomial errors.

value of 1.9×10^8 yr. There are three major differences between Bird et al. (2008) and this work that together account for this difference. The first is that the FR IIs in the Bird et al. (2008) sample were selected from a catalog of galaxy groups rather than galaxy clusters. Since the host group richness was much smaller, Bird et al. (2008) took the χ_1 ICM model as their default rather than the χ_3 model, which has a factor of two larger density parameter. The second major difference is that Bird et al. (2008) assumed jet power distributions drawn from the literature rather than deriving the jet power distribution from their (smaller) sample. Bird et al. (2008) used jet power distributions from Blundell et al. (1999) and Sadler et al. (2002) and found that the lifetime is insensitive to these two choices. This is because the lifetime calculation depends more strongly on the median value of the jet power distribution than on the higher-order moments; since

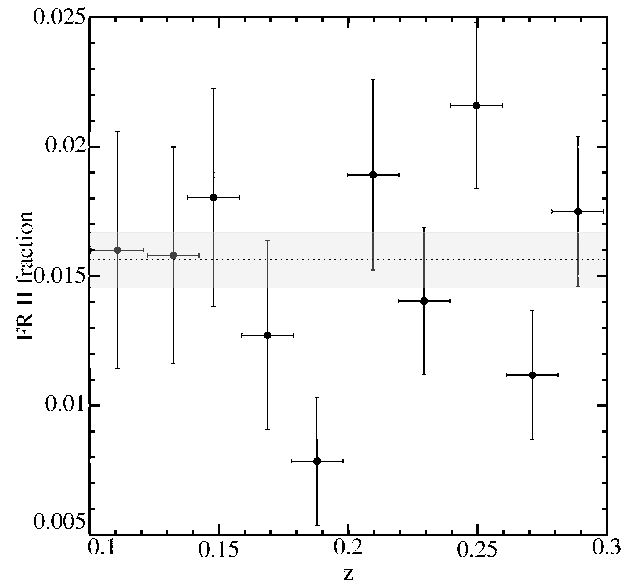


FIG. 19.— The FR II fraction of the volume-limited sample across the redshift range of the MaxBCG catalog. Horizontal error bars reflect bin widths and vertical error bars reflect the binomial error on the FR II fraction in each bin. The mean FR II fraction across the entire sample is shown by the dotted line with its binomial error represented by the shaded region. There is no evolution in the FR II fraction over the redshift range of the MaxBCG catalog.

the Blundell and Sadler distributions have similar median powers, Bird et al. (2008) point out that it is unsurprising that the two distributions produce similar lifetimes despite their different shapes. However, these distributions were derived from samples of much more luminous FR IIs than those in either the Bird et al. (2008) sample or our own; FR IIs in Blundell et al. (1999) were selected from the 3C, 6C, and 7C catalogs and the Sadler et al. (2002) distribution was derived from the bright end of the luminosity function. Consequently, Bird et al. (2008) overestimated the median jet powers of the FR IIs in their sample by approximately two orders of magnitude, and this led to an underestimate of the lifetime by a factor of approximately five. The final difference between the two studies is our use of an updated coefficient c_1 to calculate the lobe length (described in detail in §3.1). The updated coefficient is smaller than the original coefficient c_1 used by Bird et al. (2008) by about 40% and this increases the lifetime estimates by about 70%. When the differences between the two studies in jet power distribution and c_1 are taken into account, they almost entirely explain the order-of-magnitude discrepancy in the lifetime measurement. The remaining difference between the two measurements is less than a factor of two and can be due to uncertainties in the two measurements, or a small intrinsic difference in the FR II lifetime from group to cluster environments, or both.

Blundell et al. (1999) estimated the maximum lifetime of FR IIs from their observed distribution in the P - D plane. They noted that if the lifetime were too short, one would predict far fewer long FR IIs than are observed and there would be a sharp maximum-size cutoff. However, if the maximum lifetime were too large, there would be no effect on the distribution of points in the P - D plane for a flux-limited sample since FR IIs above the true maximum lifetime would generally fall below the flux limit; larger maximum lifetimes only decrease the predicted detection fraction. Blundell et al. (1999) found that the smallest maximum lifetime consistent with their observations was 5×10^8 yr, in reasonable agreement with our

value. The similarities in these lifetime estimates are interesting because our study probes FR IIs with jet powers approximately two orders of magnitude below those in the sample of Blundell et al. (1999). Wang & Kaiser (2008) fit a very similar sample with a typical maximum lifetime of a few $\times 10^7$ yr, although that choice was motivated by the Bird et al. (2008) value.

O’Dea et al. (2009) found FR II lifetimes of a few $\times 10^{6-7}$ yr with the spectral index gradient method (Leahy et al. 1989). They used a sample of 31 FR IIs at the high end of the FR II luminosity function (all of the FR IIs in their sample are in the 3C catalog), whereas sources in our sample are typically at much lower luminosities. As they note, because their flux-limited sample only includes the most powerful sources at high redshift, these sources are expected to have the smallest lifetimes. The observed expansion velocities of the sources in the O’Dea et al. (2009) sample are larger than the expansion velocities observed in our sample by about two orders of magnitude. This difference does not appear to be due to differences in the two methods, however, since we obtain expansion velocities consistent with those found by O’Dea et al. (2009) when we apply the KDA model to the sources in their sample. This suggests that the discrepancy in the lifetime measurements between our work and O’Dea et al. (2009) is due to the difference in jet powers between the two samples rather than systematic discrepancies between the two methods.

Additionally, Wang et al. (2011) found that the length of FR IIs is limited to a maximum value by the entrainment of gas within the lobe. Wang et al. (2011) argued that beyond this maximum length the radio jet is disrupted, transforming the FR II into an FR I. Because more powerful jets reach this maximum length more quickly, lifetime studies at the high end of the FR II luminosity function may systematically find lower lifetimes.

6.2. FR IIs as Sources of Heating in the ICM

An outstanding problem in high-mass galaxy formation is the suppression of substantial gas cooling. As BCGs are almost always at the centers of galaxy clusters, cool gas from the surrounding ICM is predicted to condense onto the BCG. Were this process to proceed uninterrupted, BCGs would grow to be much larger than observed. To quench these cooling flows, some mechanism must exist to heat the ICM.

To first approximation, the heating of the ICM due to a radio lobe is simply the enthalpy of the system,

$$H = \frac{\gamma}{\gamma-1} f p V, \quad (9)$$

where γ is the adiabatic index, V is the volume of the lobe, p is the pressure of the ICM immediately outside the lobe, and f is an ad hoc uncertainty factor (Bîrzan et al. 2004; Best et al. 2007). Although we do not know the pressure of the ICM outside the lobe, the KDA model does provide the pressure inside the lobe (equation A4 of Kaiser & Best, 2007). Since it is reasonable to assume that the lobe is overpressured relative to the ICM, we calculate the enthalpy of the system with the lobe pressure and thereby obtain an upper limit.

To calculate the volume of the lobe, we assume a cylindrical geometry with length l and an axial ratio of $A = 4$. The observed lengths of the FR IIs are all extended by a factor of $\pi/4$ to correct for projection effects. Finally, since the gas is relativistic, $\gamma = 4/3$. The enthalpy is therefore

$$H = \frac{256 p l^3}{\pi^2 A^2} f. \quad (10)$$

We use the KDA model to calculate the lobe pressure for every FR II in our sample based on the estimated ages and powers of the jets (see §3.3). Although we may derive a lower limit on the total ICM heating due to the adiabatic expansion of the lobe by dividing the enthalpy by the estimated age of the FR II, such an estimate is only partially useful in determining whether FR IIs can quench cooling flows in galaxy clusters. To be a successful mechanism to quench cooling flows, FR IIs must not only provide a sufficient amount of total heat, but must also provide a sufficient amount of heat throughout the central region of the cluster. Otherwise, cooling flows would be quenched in some regions and would proceed unabated in others. In particular, if gas on the equatorial plane between the two lobes is not shocked, the assumption that the lobe expands adiabatically will provide an upper limit on the heating of gas in this region.

To determine whether ICM heating from the adiabatic expansion of the lobe is sufficient to halt substantial gas cooling, we compare the average heating rate to the average cooling of the ICM. While we do not have X-ray luminosities to directly estimate cooling rates, we can estimate the typical cooling rate from the scaling relation between X-ray luminosity and cluster velocity dispersion of

$$\log_{10}(L_{45}) = -1.34 + 2.0 \times \log_{10}(\sigma_{500}) \text{ erg s}^{-1}, \quad (11)$$

where L_{45} is the X-ray luminosity in units of 10^{45} erg s^{-1} and σ_{500} is the cluster velocity dispersion in units of 500 km s^{-1} (Ortiz-Gil et al. 2004). We estimate the cluster velocity dispersions from the scaling relation measured by Becker et al. (2007) of

$$\langle \ln \sigma \rangle = 6.17 + 0.436 \ln N_{\text{gal}}^{200} / 25. \quad (12)$$

These two equations provide an estimate of the ICM cooling in the MaxBCG clusters. The heating rate from the enthalpy of the lobes (assuming $f = 1$) is shown with the estimated cooling rate in Figure 20. The typical heating rate due to the FR II lobes is at least an order of magnitude smaller than the estimated cooling rate, implying that heating from radio-mode feedback from FR IIs is insufficient to quench cooling flows in rich clusters. Figure 20 also demonstrates that the total jet powers exceed the amount required to counteract cooling by approximately an order of magnitude. That is, only $\sim 10\%$ of the jet power is needed to counteract the predicted cooling, while only $\sim 1\%$ of the jet power appears to contribute to the enthalpy of the lobes. These jets are consequently sufficiently powerful to counteract cooling in individual clusters, but this power may not couple to the ICM.

There are several sources of uncertainty in the enthalpy calculation that may bring the heating and cooling rates into better agreement. First, our calculation of the enthalpy of the lobe requires knowledge of the axial ratio of the lobe. We assume an axial ratio of $A = 4$, but because $H \propto A^{-2}$, an overestimate of the axial ratio will lead to an underestimate of the enthalpy. However, the axial ratio can generally be no smaller than $A = 2$, which corresponds to spherical lobes. This would increase the enthalpy by a factor of four.

Second, our calculation of the enthalpy of the lobe requires knowledge of the pressure within the lobe. This can be calculated from the KDA model, but is dependent upon the density of the ICM outside the lobe. Specifically, if the density profile of the ICM has a power-law slope of $\beta = 2$, $p \propto \rho t^{-2}$, where t is the lifetime of the FR II (Kaiser & Best 2007). Since $t \propto \rho^{1/3}$, we have that $p \propto \rho^{1/3}$. The enthalpy is proportional to pV , but the volume of the lobe is an observable and is therefore

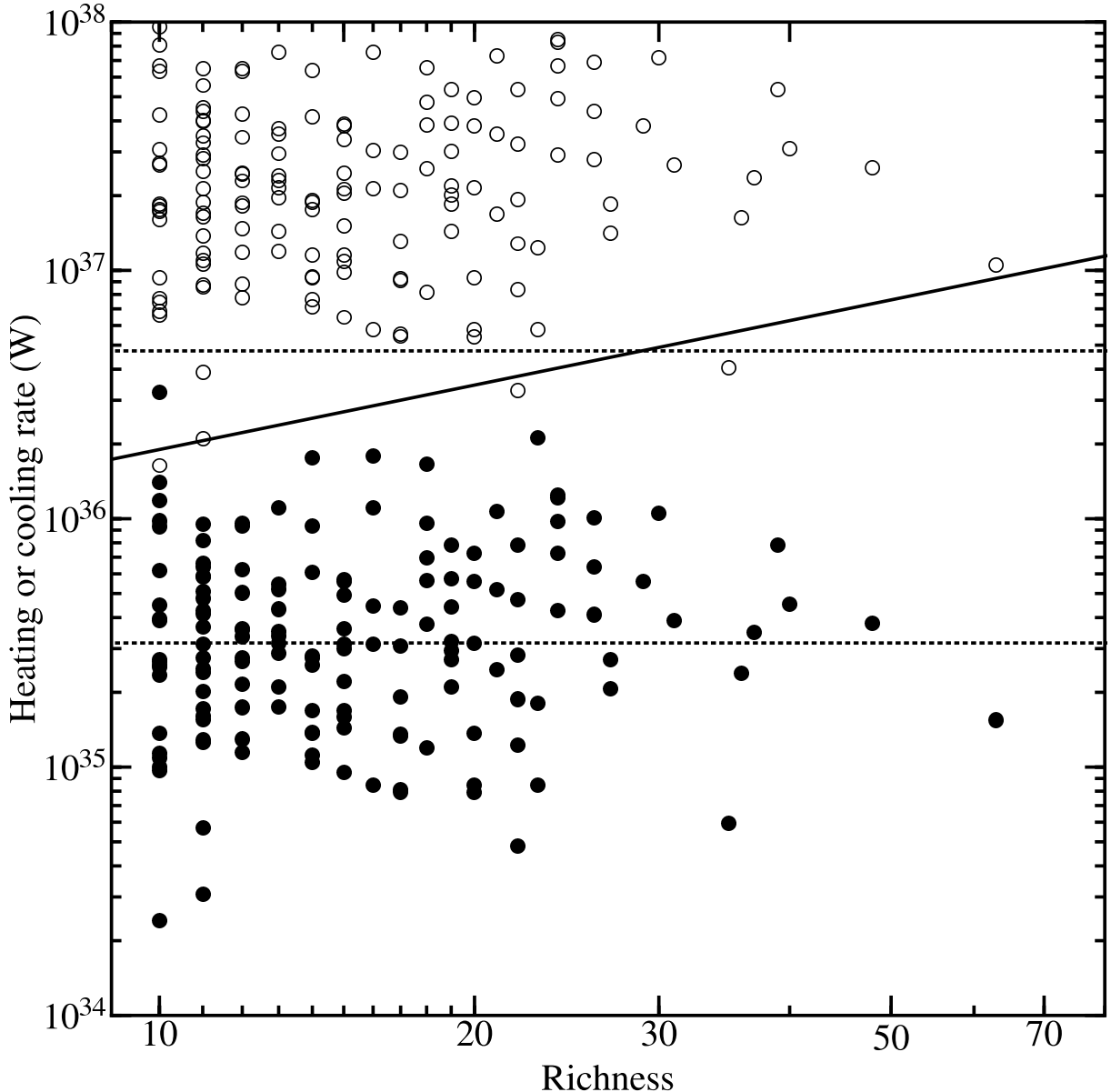


FIG. 20.— The estimated ICM heating rates due to FR IIs (filled circles) and the estimated ICM cooling rates (solid line). The heating rates represent the enthalpy of each FR II in our sample divided by the age of the FR II. Since the enthalpy is calculated from the pressure inside the lobe rather than the external pressure, these points are upper limits on the average heating rate. The cooling rate (solid line) is calculated by combining the scaling relation between X-ray luminosity and velocity dispersion from Ortiz-Gil et al. (2004) with the scaling relation between velocity dispersion and cluster richness from Becker et al. (2007). (A similar figure by Best et al. 2007 included several other scaling relations between X-ray luminosity and velocity dispersion; since these are all very similar to the Ortiz-Gil relation, they are omitted here for clarity.) The jet powers (open circles) are higher than the required cooling rate, but only $\sim 1\%$ of this power generates the enthalpy of the lobe. Approximately 10% of the jet power is needed to balance cooling. (For comparison, the open circles represent the jet powers of the FR IIs in our sample, estimated in §3.3). The lower dotted line represents the median heating of FR IIs in our sample assuming an uncertainty factor of $f = 1$ (i.e. assuming that our estimate of the ICM heating is exactly equal to the true ICM heating). The upper dotted line represents the median ICM heating assuming an uncertainty factor of $f = 15$. This is approximately the value of f required for FR II heating to balance the ICM cooling.

independent of our assumptions about the ICM density. Thus,

$$H \propto \rho^{1/3}. \quad (13)$$

If the density profile does not have a power-law slope of $\beta = 2$, there will be an additional dependence of the enthalpy on the jet power, but if the slope is nearly 2, the deviation from the above relationship will be small. We therefore expect the dependence of the enthalpy on the ICM density assumption to be weak. If the typical ICM density is $5.9 \times 10^{-24} \text{ kg m}^{-3}$ at 260 kpc (the largest density we use in this paper), rather than our assumed value of $7.2 \times 10^{-26} \text{ kg m}^{-3}$ at 391 kpc, the enthalpy increases by only a factor of 3.

With a similar enthalpy analysis, Best et al. (2007) found that radio-mode feedback has particular difficulty quenching

cooling flows in very rich clusters. They estimated the average ICM heating due to the AGN with a power-law relationship between radio luminosity and jet power from Best et al. (2006). Best et al. (2007) compared this heating rate to the expected cooling rate estimated from several generic scaling relations between X-ray luminosity and velocity dispersion and found that the estimated heating rate fell below the cooling rate derived from the X-ray luminosity for clusters with a velocity dispersion above $\sigma_v \gtrsim 300 \text{ km s}^{-1}$. All of the MaxBCG clusters are expected to be above this velocity dispersion.

Best et al. (2007) identified three major sources of uncertainty in their analysis: (1) the conversion from radio luminosity to jet power, (2) the estimate of the ICM heating from

the jet power, and (3) the fraction of ICM heating that takes place within the cooling radius. They parametrized these uncertainties by the ad hoc uncertainty factor, f , in Equation 10. An uncertainty factor of $f = 1$ implies that the ICM heating within the cooling radius is exactly the amount that Best et al. (2007) infer from the radio luminosities. Larger values of f correspond to more ICM heating within the cooling radius than predicted, and smaller values correspond to less heating. Although Best et al. (2007) argue that f is likely close to unity, they note that if f is somewhat larger than 10 then the ICM heating due to radio-mode feedback would be sufficient to quench cooling flows in nearly all galaxy clusters. A better constraint on f could therefore determine whether radio-mode feedback is a viable mechanism to quench cooling flows in rich clusters. Because our approach takes observed FR II lengths and radio luminosities and uses an FR II evolution model to constrain the jet power distribution of our sample, we have effectively removed the first source of uncertainty from f .

As noted by Best et al. (2007), there is additional uncertainty in the fraction of the heating that takes place within the cooling radius. We have assumed that all of it does, but this fraction could be much less than 1. If this fraction is small, however, it becomes yet more difficult for radio-mode feedback to quench cooling flows in rich clusters.

Our results shown in Figure 20 are similar to those of Best et al. (2007)—radio-mode feedback can only quench cooling flows in rich clusters ($N_{200} \geq 10$) if the uncertainty factor satisfies $f \gtrsim 15$. Meeting this criterion requires that the cores of galaxy clusters be much denser than expected, that FR II lobes be nearly spherical, and that the ICM be only slightly underpressured relative to the lobe. This strongly constrains the environments in which radio-mode feedback is an effective mechanism to quench cooling flows.

Even if $f \gtrsim 15$, our duty cycle calculation suggests that FR IIs can be an effective ICM heating mechanism for only a small fraction of the cluster’s lifetime. As described in detail in §4.4, only $\sim 2\%$ of the BCGs in the MaxBCG catalog have FR IIs after the correction for selection effects. If every BCG in the MaxBCG catalog is as likely to host an FR II as any other (a reasonable assumption given the similarity between the vast majority of MaxBCG clusters in redshift and richness), then FR IIs are powered for $\sim 2\%$ of the cluster’s lifetime. If the uncertainty factor f were greater than ~ 15 , FR IIs would be able to quench cooling flows during this $\sim 2\%$ of the cluster’s lifetime, but would be unable to quench cooling flows at any other time. For FR IIs to heat the ICM sufficiently to quench cooling flows for a substantial fraction of the cluster’s lifetime would require the uncertainty factor to be yet an order of magnitude larger. Since we have largely eliminated the source of uncertainty (1) of the conversion from radio luminosity to jet power, and the source of uncertainty (3) of the fraction of ICM heating that takes place within the cooling radius only acts to make f smaller, the only way to increase f is in the source of uncertainty (2) of the estimate of the ICM heating from the jet power. One way to increase f is if there were heating due to shocks near the cluster center, as our calculations have only included ICM heating due to adiabatic expansion.

Another possible solution that addresses both the apparently small value of f and the low duty cycle is if the FR II continues to affect the ICM after the radio source is no longer apparent. Hydrodynamical simulations by ? indicate that FR IIs can substantially effect the cooling properties of the

ICM for significant period of time (up to an order of magnitude longer than the lifetime of the jet) after the jet has turned off by removing gas that otherwise would have cooled on longer timescales. Given a longer period of time in which to couple to the external gas, FR IIs could be more efficient than their lifetime alone suggests. Our results therefore imply that if FR IIs are major sources of heating in galaxy clusters, they contribute the vast majority of this heating after their demise.

The range of jet powers of these FR IIs provides some potential constraints on the jet powers in the additional 20% of the BCGs in the MaxBCG catalog that host other cluster radio sources. The two most likely scenarios for why these other sources do not exhibit an FR II morphology are that they fall below the critical jet power criterion (e.g., Kaiser & Best 2007) and that local variations in the ICM have disrupted their jets. With the notable exception of Cygnus A (Carilli et al. 1994), nearly all of the early evidence for the impact of radio sources on the ICM came from FR Is such as Perseus A (Boehringer et al. 1993; Fabian et al. 2000) and Hydra A (McNamara et al. 2000). If the vast majority of cluster radio sources are not FR IIs because they are insufficiently powerful, then their jet powers must fall below the FR IIs in our sample, or $\lesssim 5 \times 10^{36}$ W. This is at the low end of the estimates of the power required to inflate cavities seen in X-ray gas of $\sim 10^{35-39}$ W (e.g., Birzan et al. 2008), although the clusters studied with X-rays may not be representative of all cluster radio galaxies.

If the jet powers for these other radio sources are below the typical FR II jet powers by only one order of magnitude, or they are jets that exceed the critical value but have been disrupted, then they will be sufficiently powerful to counteract cooling in their clusters. The first scenario would require the coupling between jet power and the ICM to be closer to 100%. The second scenario could be constrained with detailed comparisons between the cavity powers and lobe enthalpies of FR Is and IIs. In addition, while our data suggest that the cavity power may be substantially less than the jet power for FR IIs, a different relation between cavity and jet power may hold for FR Is. If they are more equal, then many FR Is may be too weak to create FR IIs. Better estimates of the environmental conditions and intrinsic properties that produce the FR I/II dichotomy would also provide valuable new constraints on the properties of the radio sources that likely ultimately produce feedback on the ICM.

7. SUMMARY

We estimate the typical lifetime, jet powers, and ages for a new sample of 151 FR IIs identified in data from the FIRST radio survey for clusters in the MaxBCG catalog of Koester et al. (2007a). We use radio luminosities, projected length measurements, and the KDA FR II model to show that the typical FR II lifetime is 1.9×10^8 yr. We find that the distribution of FR II jet power in BCGs is best described by a log-normal distribution rather than a power-law distribution as has been previously assumed. We furthermore find that the jet power estimated for FR IIs in our sample is lower than that of other samples (e.g., Kaiser & Best 2007; Bird et al. 2008). The major uncertainties in the jet power and lifetime measurements are the density of the ICM and the axial ratio of the jets. Reasonable ranges in ICM density and axial ratio affect the lifetime estimate at the factor of two level.

We examine the relationship between the properties of FR IIs and the properties of BCGs and the clusters. We find that while BCG luminosity is correlated with FR II jet power,

other cluster properties such as BCG velocity dispersion and cluster richness are not strongly correlated with either the jet power or the FR II lifetime. These results suggest that the intrinsic properties of FR IIs are not highly dependent on their larger-scale environment.

We evaluate the heating of the ICM from FR IIs in galaxy clusters assuming adiabatic expansion of overpressured radio lobes. The time-averaged enthalpy of the lobes implies that ICM heating due to FR IIs is smaller than ICM cooling by over an order of magnitude. Although the jet provides the lobe with a sufficient amount of energy to quench cooling flows, FR IIs cannot be major contributors to ICM heating without a viable mechanism by which this energy can be distributed throughout the ICM. This stands in stark contrast to the total jet power, which *exceeds* the cooling rate by approximately an order of magnitude. If the jet power could couple with the ICM with $\sim 10\%$ efficiency, this would suffice to counteract cooling, albeit for only the $\sim 2\%$ of BCGs that host an FR II. The larger fraction of other radio sources in BCGs may be lower-power jets that are insufficiently overpressured to form an FR II morphology. These sources would require nearly 100% coupling efficiency to the ICM and jet powers only an order of magnitude below our sample to balance cooling.

We would like to thank Brian McNamara, Chris O’Dea, Yang Wang, and the anonymous referee for helpful comments on the manuscript. We would also like to thank Scott Gaudi for providing useful suggestions and acknowledge Benjamin Shappee for discussing the manuscript with JMA.

This research makes use of the FIRST and NVSS radio surveys. The National Radio Astronomy Observatory is a facility of the National Science Foundation operated under cooperative agreement by Associated Universities, Inc. The Cosmology Calculator by Wright (2006) was used in the preparation of this paper.

Funding for the SDSS and SDSS-II has been provided by the Alfred P. Sloan Foundation, the Participating Institutions, the National Science Foundation, the U.S. Department of Energy, the National Aeronautics and Space Administration, the Japanese Monbukagakusho, the Max Planck Society, and the Higher Education Funding Council for England. The SDSS Web Site is <http://www.sdss.org/>.

The SDSS is managed by the Astrophysical Research Consortium for the Participating Institutions. The Participating Institutions are the American Museum of Natural History, Astrophysical Institute Potsdam, University of Basel, University of Cambridge, Case Western Reserve University, University of Chicago, Drexel University, Fermilab, the Institute for Advanced Study, the Japan Participation Group, Johns Hopkins University, the Joint Institute for Nuclear Astrophysics, the Kavli Institute for Particle Astrophysics and Cosmology, the Korean Scientist Group, the Chinese Academy of Sciences (LAMOST), Los Alamos National Laboratory, the Max-Planck-Institute for Astronomy (MPIA), the Max-Planck-Institute for Astrophysics (MPA), New Mexico State University, Ohio State University, University of Pittsburgh, University of Portsmouth, Princeton University, the United States Naval Observatory, and the University of Washington.

REFERENCES

- Allen, S. W., Dunn, R. J. H., Fabian, A. C., Taylor, G. B., & Reynolds, C. S. 2006, *MNRAS*, 372, 21
- Barai, P., & Wiita, P. J. 2006, *MNRAS*, 372, 381
- Becker, M. R., et al. 2007, *ApJ*, 669, 905
- Becker, R. H., White, R. L., & Helfand, D. J. 1995, *ApJ*, 450, 559
- Berlind, A. A., et al. 2006, *ApJS*, 167, 1
- Best, P. N., Kaiser, C. R., Heckman, T. M., & Kauffmann, G. 2006, *MNRAS*, 368, L67
- Best, P. N., Kauffmann, G., Heckman, T. M., Brinchmann, J., Charlot, S., Ivezić, Ž., & White, S. D. M. 2005, *MNRAS*, 362, 25
- Best, P. N., von der Linden, A., Kauffmann, G., Heckman, T. M., & Kaiser, C. R. 2007, *MNRAS*, 379, 894
- Bicknell, G. V., Dopita, M. A., & O’Dea, C. P. O. 1997, *ApJ*, 485, 112
- Bird, J., Martini, P., & Kaiser, C. 2008, *ApJ*, 676, 147
- Birzan, L., McNamara, B. R., Nulsen, P. E. J., Carilli, C. L., & Wise, M. W. 2008, *ApJ*, 686, 859
- Birzan, L., Rafferty, D. A., McNamara, B. R., Wise, M. W., & Nulsen, P. E. J. 2004, *ApJ*, 607, 800
- Blandford, R. D., & Znajek, R. L. 1977, *MNRAS*, 179, 433
- Blundell, K. M., Rawlings, S., & Willott, C. J. 1999, *AJ*, 117, 677
- Boehringer, H., Voges, W., Fabian, A. C., Edge, A. C., & Neumann, D. M. 1993, *MNRAS*, 264, L25
- Braude, S. Y., Lebedeva, O. M., Megn, A. V., Ryabov, B. P., & Zhouck, I. N. 1969, *MNRAS*, 143, 289
- Burns, J. O. 1990, *AJ*, 99, 14
- Canizares, C. R., Fabbiano, G., & Trinchieri, G. 1987, *ApJ*, 312, 503
- Carilli, C. L., Perley, R. A., & Harris, D. E. 1994, *MNRAS*, 270, 173
- Carlborg, R. G., Yee, H. K. C., & Ellingson, E. 1997, *ApJ*, 478, 462
- Carvalho, J. C., & O’Dea, C. P. 2002a, *ApJS*, 141, 337
- . 2002b, *ApJS*, 141, 371
- Cavagnolo, K. W., McNamara, B. R., Nulsen, P. E. J., Carilli, C. L., Jones, C., & Birzan, L. 2010, *ApJ*, 720, 1066
- Condon, J. J., Cotton, W. D., Greisen, E. W., Yin, Q. F., Perley, R. A., Taylor, G. B., & Broderick, J. J. 1998, *AJ*, 115, 1693
- Cotter, G. 1996, PhD thesis, University of Cambridge
- Cotter, G., Rawlings, S., & Saunders, R. 1996, *MNRAS*, 281, 1081
- Dolag, K., Jubelgas, M., Springel, V., Borgani, S., & Rasia, E. 2004, *ApJ*, 606, L97
- Faber, S. M., & Jackson, R. E. 1976, *ApJ*, 204, 668
- Fabian, A. C. 1994, *ARA&A*, 32, 277
- Fabian, A. C., Reynolds, C. S., Taylor, G. B., & Dunn, R. J. H. 2005, *MNRAS*, 363, 891
- Fabian, A. C., et al. 2000, *MNRAS*, 318, L65
- Falle, S. A. E. G. 1991, *MNRAS*, 250, 581
- Fanaroff, B. L., & Riley, J. M. 1974, *MNRAS*, 167, 31P
- Forman, W., et al. 2005, *ApJ*, 635, 894
- Freeland, E., & Wilcots, E. 2011, *ApJ*, 738, 145
- Garrington, S. T., & Conway, R. G. 1991, *MNRAS*, 250, 198
- Gopal-Krishna, & Wiita, P. J. 2000, *A&A*, 363, 507
- Gültekin, K., et al. 2009, *ApJ*, 698, 198
- Ito, H., Kino, M., Kawakatu, N., Isobe, N., & Yamada, S. 2008, *ApJ*, 685, 828
- Jetha, N. N., Ponman, T. J., Hardcastle, M. J., & Croston, J. H. 2007, *MNRAS*, 376, 193
- Jones, C., & Forman, W. 1984, *ApJ*, 276, 38
- Jones, C., Forman, W., Vikhlinin, A., Markevitch, M., David, L., Warmflash, A., Murray, S., & Nulsen, P. E. J. 2002, *ApJ*, 567, L115
- Kaiser, C. R., & Alexander, P. 1997, *MNRAS*, 286, 215
- . 1999a, *MNRAS*, 305, 707
- . 1999b, *MNRAS*, 302, 515
- Kaiser, C. R., & Best, P. N. 2007, *MNRAS*, 381, 1548
- Kaiser, C. R., Dennett-Thorpe, J., & Alexander, P. 1997, *MNRAS*, 292, 723
- Kino, M., & Kawakatu, N. 2005, *MNRAS*, 364, 659
- Koester, B. P., et al. 2007a, *ApJ*, 660, 239
- . 2007b, *ApJ*, 660, 221
- Laing, R. A., Riley, J. M., & Longair, M. S. 1983, *MNRAS*, 204, 151
- Leahy, J. P., Muxlow, T. W. B., & Stephens, P. W. 1989, *MNRAS*, 239, 401
- Leahy, J. P., & Williams, A. G. 1984, *MNRAS*, 210, 929
- Ledlow, M. J., & Owen, F. N. 1996, *AJ*, 112, 9
- Machalski, J., Chyzy, K. T., & Jamroz, M. 2004, *AcA*, 54, 249
- Manolakou, K., & Kirk, J. G. 2002, *A&A*, 391, 127
- Martini, P. 2004, *Coevolution of Black Holes and Galaxies*, 169
- Mathews, W. G. 2009, *ApJ*, 695, L49
- McNamara, B. R., & Nulsen, P. E. J. 2007, *ARA&A*, 45, 117
- McNamara, B. R., Rohanizadegan, M., & Nulsen, P. E. J. 2011, *ApJ*, 727, 39
- McNamara, B. R., et al. 2000, *ApJ*, 534, L135
- Mohr, J. J., Mathiesen, B., & Evrard, A. E. 1999, *ApJ*, 517, 627
- Mulchaey, J. S. 2000, *ARA&A*, 38, 289

- Novak, G. S., Faber, S. M., & Dekel, A. 2006, *ApJ*, 637, 96
- O'Dea, C. P., Daly, R. A., Kharb, P., Freeman, K. A., & Baum, S. A. 2009, *A&A*, 494, 471
- Ortiz-Gil, A., Guzzo, L., Schuecker, P., Böhringer, H., & Collins, C. A. 2004, *MNRAS*, 348, 325
- Pearson, K. 1895, *Proc. R. Soc. Lond.*, 58, 240
- Peterson, J. R., et al. 2001, *A&A*, 365, L104
- Punsly, B. 2005, *ApJ*, 623, L9
- Punsly, B., & Zhang, S. 2011, *ApJ*, 735, L3+
- Rafferty, D. A., McNamara, B. R., Nulsen, P. E. J., & Wise, M. W. 2006, *ApJ*, 652, 216
- Sadler, E. M., et al. 2002, *MNRAS*, 329, 227
- Scheuer, P. A. G. 1995, *MNRAS*, 277, 331
- Sheldon, E. S., et al. 2009, *ApJ*, 703, 2232
- Subrahmanyam, R., Saripalli, L., & Hunstead, R. W. 1996, *MNRAS*, 279, 257
- Tamura, T., et al. 2001, *A&A*, 365, L87
- Vikhlinin, A., Kravtsov, A., Forman, W., Jones, C., Markevitch, M., Murray, S. S., & Van Speybroeck, L. 2006, *ApJ*, 640, 691
- Wang, Y., & Kaiser, C. R. 2008, *MNRAS*, 388, 677
- Wang, Y., Knigge, C., Croston, J. H., & Pavlovski, G. 2011, *MNRAS*, 418, 1138
- White, R. L., Becker, R. H., Helfand, D. J., & Gregg, M. D. 1997, *ApJ*, 475, 479
- White, S. D. M., & Frenk, C. S. 1991, *ApJ*, 379, 52
- Willott, C. J., Rawlings, S., Blundell, K. M., & Lacy, M. 1999, *MNRAS*, 309, 1017
- Wright, E. L. 2006, *PASP*, 118, 1711